Impact of an Antifungal Insect Defensin on the Proteome of the Phytopathogenic Fungus Botrytis cinerea

Thomas Aumer, Sébastien N Voisin, Thomas Knobloch, Celine Landon, Philippe Bulet

Impact of an antifungal insect defensin on the proteome of the phytopathogenic fungus *Botrytis cinerea*

Thomas Aumer[1], *Sébastien N. Voisin*[2], *Thomas Knobloch*[3], *Céline Landon*[4], *Philippe Bulet*[1,2*]

[1] CR Université Grenoble Alpes, Institute for Advanced Biosciences, Inserm U1209, CNRS UMR 5309, Grenoble, France

[2] Plateforme BioPark d'Archamps, Archamps Technopole, Saint Julien en Genevois, France

[3] Bayer SAS, Bayer CropScience, Centre de Recherche de la Dargoire, Lyon, France

[4] Centre de Biophysique Moléculaire, CNRS UPR 4301, Orléans, France

*** Corresponding Author**

Dr Philippe Bulet

Plateforme BioPark d'Archamps, Bât. Le Forum 1, 260 Avenue Marie Curie, Archamps Technopole, Saint Julien en Genevois Cedex, France

E-mail address: philippe.bulet@univ-grenoble-alpes.fr, philippe.bulet@biopark-archamps.org

ABSTRACT

ETD151, an analogue of the antifungal insect defensin heliomicin, is an antifungal peptide active against yeasts and filamentous fungi. In order to decipher the mechanisms underlying its molecular action on the phytopathogenic fungus *Botrytis cinerea*, a necrotrophic pathogen responsible for gray mold disease, we investigated the changes in three-day old mycelia upon treatment with different concentrations of ETD151. Optical and fluorescent microscopies were used prior to establishing the peptide/protein profiles through two mass spectrometry approaches: MALDI profiling, to generate molecular mass fingerprints as peptide signatures, and a gel-free bottom-up proteomics approach. Our results show that a concentration of ETD151 above the half-maximal inhibitory concentration can alter the integrity of the mycelial structure of *B. cinerea*. Furthermore, reproducible modifications of the peptide/protein composition were demonstrated in the presence of ETD151 within a 1.5-16 kDa mass range. After the robustness of LC-ESI-MS/MS analysis on *B. cinerea* mycelial extracts was confirmed, our analyses highlighted 340 significantly modulated proteins upon treatment with ETD151 within a 4.8-466 kDa mass range. Finally, data mapping on KEGG pathways revealed the molecular impact of ETD151 on at least six pathways. In particular, for the effect on oxidative phosphorylation, we clearly demonstrated that ETD151 does not interact directly with the mitochondrial respiratory chain.

Keywords: Insect defensin, antifungal defensin, *Botrytis cinerea*, proteomics, fungal infection, heliomicin, mechanism of action

INTRODUCTION

Phytopathogenic fungi are a major concern for crops in agriculture. In the last decade, phytopathology experts have alerted the scientific community to several species threatening food security and biodiversity[1]. Every year, fungal pathogens destroy more than 125 million tons of the world's top five major crops[2]: rice (rice blast caused by *Magnaporthe oryzae*), wheat (rust caused by *Puccinia graminis*), maize (smut caused by *Ustilago maydis*), potatoes (late blight caused by *Phytophthora infestans*) and soybean (rust caused by *Phakospora pachyrhizi*). These production losses could feed an additional 600 million people per year. Among the phytopathogenic fungi, *Botrytis cinerea* (teleomorph *Botryotinia fuckeliana*) is a necrotrophic pathogen responsible for gray mold disease causing significant crop losses in more than 200 plant species worldwide[3,4]. Ranked scientifically and economically as the second most important fungal pathogen by the international phytopathological community[5], *B. cinerea* generates significant costs over a broad host range. Damage occurs in different stages of fruit and vegetable production in open fields or in greenhouses and requires extensive disease control, mainly by fungicide application. Concerns about this fungus have also increased due to the recent discovery of *B. cinerea* fungicide-resistant strains in field populations[6]. The introduction of site-specific fungicides almost 50 years ago revolutionized crop protection and has remained until now the main approach for reducing fungal disease progression. However, plant pathogenic fungi can adapt, leading to a tremendous loss of plant protection effectiveness. Fungicide resistant pathogens have emerged over time and spread globally[7]. Most important classes of antifungals (e. g. benzimidazoles, strobilurins, hydroxyanilides) are concerned by the development of resistance compromising the efficacy of crop protection. As a new major

challenge, it is necessary to propose novel fungicides with innovative mechanisms of action or alternative strategies with non-chemical products[8].

Scientists are investigating the field of antimicrobial peptides (AMPs), looking for new molecules with novel targets, reduced toxicity and broad-spectrum activity for a low-rate use. Also known as host defense peptides (HDPs), AMPs are key components of the innate immune system of all organisms, protecting them against attacks by invading pathogens and stressors[9]. Even if a wide range of AMPs have been identified, they can be globally classified according to their amino acid composition, their structure and the organization of their disulfide bonds. One of these classes, the CSαβ-defensins (Cysteine-stabilized α-helix β-sheet), groups small, cationic, cysteine-rich peptides with specific 3D organization and conserved disulfide bridge arrays[10–12]. Intriguingly, the CSαβ-defensins have been found in plants and insects. Plant defensins are well-known and extensively studied for their antifungal activity[13]. On the contrary, only a few insect defensins have been reported to be exclusively antifungal, most of them exhibiting antimicrobial activities (antibacterial and antifungal), with particular efficacy against Gram-positive bacteria[14]. The first antifungal insect defensin to be described was drosomycin[15,16] from the fruit fly *Drosophila melanogaster* (Diptera). It was followed by heliomicin[17,18] from the tobacco budworm *Heliothis virescens* (Lepidoptera), termicin[19,20] from *Pseudacanthotermes spiniger* (Isoptera), gallerimycin[21] from the great wax moth larvae *Galleria mellonella* (Lepidoptera) and ARD1[22] from the larvae of *Archaeoprepona demophon* (Lepidoptera).

The promising *in vitro* antifungal activity of insect defensins against plant or human pathogens, as well as their non-cytotoxicity, highlights their potential as candidates for crop protection strategies[23] and/or therapeutic applications[24]. In the 2000s, the French biotechnology company EntoMed SA was the first to develop natural insect AMPs for the treatment of systemic

fungal infections affecting immunocompromised patients[25]. Heliomicin was the working model of a cutting-edge optimization program based on phylogenic exploration and fine-tuned mutagenesis. The results of their work, a 44 amino acid peptide, called ETD151, revealed enhanced antifungal activity against *Candida albicans* and *Aspergillus fumigatus* as well as additional activity against *Cryptococcus neoformans,* as compared to heliomicin[22]. ETD151 was the principal product developed by EntoMed SA for treating antifungal infections[26].

However, limited data has been gathered on the antifungal mechanism of action of insect defensins, which include the inhibition of spore germination, the alteration of germ tube elongation and the release of cytoplasmic content[23,27]. Comparisons based on structural analysis and activity tests on fungal mutants, provided evidence of mechanical commonalities between heliomicin, drosomycin and some antifungal plant defensins such as the radish defensin RsAFP2[28–30]. In contrast to insect defensins, the mechanisms of action of plant defensins have been widely investigated. In most cases, the first step is the interaction with non-protein fungal membrane partners such as sphingolipids or phospholipids[31]. Thereafter, plant defensins can either be internalized or remain outside the fungal cells. Cell death can occur via multiple mechanisms, induction of fungal membrane permeabilization, reactive oxygen species (ROS), apoptosis, or mitochondrial functionality loss[32]. Effects differ depending on the target organism; the mechanisms of action of the *Medicago* spp. defensin MtDef4 against the ascomycete fungi *Neurospora crassa* and *Fusarium graminearum*[33] are not the same. Upon exposure to antifungal plant defensins, fungal cells will induce mechanisms to defend themselves against these adverse effects. A family of conserved kinases, MAPK, regulate tolerance to plant defensins. In yeast, the MAPK pathways are involved in filamentous growth, cell wall integrity (CWI) and the high osmolarity/glycerol (HOG) response[34]. All of these elements provide a background for studying

105 the mode of action of ETD151, an optimized peptide analogue of the two lepidopteran insect
106 antifungal peptides heliomicin and ARD1.

107 To decipher the mechanism of action of ETD151 on the fungal phytopathogen *B. cinerea*, a
108 proteomics approach based on matrix-assisted laser desorption/ionization mass spectrometry
109 (MALDI-MS) and liquid chromatography-mass spectrometry coupled to electrospray ionization
110 (ESI-LC-MS) was used. The elucidation of the *B. cinerea* genome was a significant
111 breakthrough for the proteomics research community and has provided for the accurate
112 identification of proteins in this fungus, mainly from mycelial samples[35–38]. In the past ten years,
113 several methodological developments and technological advances in *Botrytis* proteomics have
114 offered effective new tools for achieving a better understanding of *B. cinerea* biology and how
115 its proteins are involved in pathogenic biological processes[39,40]. Most of this work focused on the
116 secretome or virulence factors produced by the fungus, like cell wall degrading enzymes,
117 considered as key elements in the different steps of the infection cycle of phytopathogenic
118 fungi[41,42].

119 Due to the dynamic nature of the proteome, the addition of an antifungal compound should
120 affect processes occurring at the surface and / or within the fungal cell[43]. In this work we compare
121 the protein profiles of extracts of fresh mycelia treated with ETD151 *vs* untreated cultures. This
122 proteomics study gives insight into the mechanism of action of this insect defensin on the fungus
123 *B. cinerea*.

124

MATERIALS AND METHODS

Chemical reagents

A liquid minimum medium based on Tanaka's medium B[44,45] and a Potato Dextrose Broth medium diluted 1:4 in water (25% PDB) were prepared using reagents from Sigma-Aldrich (St. Louis, MO, USA). Potato Dextrose Agar (PDA) was purchased from Oxoid (Basingstoke, UK). The reagents α-cyano-4-hydroxycinnamic acid (4-HCCA), ammonium bicarbonate (ABC), dithiothreitol (DTT), iodoacetamide (IAA), HPLC-grade dimethyl sulfoxide (DMSO) and LC-MS-grade formic acid (FA) were from Sigma-Aldrich. SYTOX Green Nucleic Acid Stain (5 mM in DMSO) was from Thermo Fisher Scientific (Waltham, MA, USA), *Rapi*Gest SF surfactant was from Waters (Milford, MA, USA) and sequencing-grade modified trypsin was from Promega (Madison, WI, USA). Acetonitrile (ACN), ethanol absolute anhydrous (EtOH), trifluoroacetic acid (TFA), all LC-MS grade quality or higher, were obtained from Carlo Erba Reagents (Val de Reuil, France). Protein Calibration Standard I (ProtMix) and Peptide Calibration Standard II (PepMix) were purchased from Bruker Daltonics (Germany). For all experiments, MilliQ water was used (Billerica, MA, USA).

Biological material

Spores of *Botrytis cinerea* isolated from the field and cryopreserved in 10% DMSO were provided by the La Dargoire Research Center (Bayer CropScience, France). All spores of *B. cinerea* used in this study were derived from the same initial batch. For each experiment, a cryotube was thawed and the stock solution of spores was diluted with sterile MilliQ water resulting in a final concentration of 1.5 x 10^5 spores per mL (sp/mL) in the presence of 0.1% DMSO. In order to have fresh fungal material, Falcon® culture petri dishes (Corning, NY, USA)

containing PDA solid medium were inoculated with 150 μL of the appropriate spore suspension. Culture dishes were left in the dark for seven days in an incubator (Memmert, Schwabach, Germany) maintained at 20°C and at 70% level of hygrometry. These parameters were defined as the culture conditions for all our experiments. To prepare a fresh spore solution, spores were harvested from one seven-day old culture dish using a Falcon® cell scraper (Corning), filtered on a Falcon® nylon 100 μm cell strainer (Corning), counted twice with a Malassez chamber and adjusted to a final concentration of 500 sp/mL in minimal medium.

Antifungal assay

The bioactive peptide ETD151, provided by Dr. Philippe Bulet, was produced by high cell density fermentation of a modified *Saccharomyces cerevisiae* strain developed by the former company EntoMed S.A. (Illkirch, France) and preserved as a stock solution in saline buffer. ETD 151 was desalted by solid phase extraction using Sep-Pak C_{18} Classic Cartridges (Waters) following the manufacturer's instructions. Solutions from 250 to 0.49 μM of ETD151 were prepared in sterile MilliQ water. Antifungal assays on *B. cinerea* were performed in sterile 96-well plates (TPP Techno Plastic Products AG, Trasadingen, Switzerland). To assess inhibition of mycelium growth, microplate wells were filled with 135 μL of the fresh suspension at 500 sp/mL prior to incubation in the conditions reported in the Biological material section. Addition of 15 μL of the ETD151 solutions, giving final concentrations of 25 to 0.049 μM, occurred three days later. The plate was gently shaken and incubated for four additional days. Evolution of the assay was monitored daily by absorbance measurement at 630 nm with an ELx808 microplate reader (BioTek, Winooski, VT, USA). The dose-response curve was generated with Microsoft Excel

software and XLfit plug-in (release 5.4). Data were adjusted according to the "Dose-response one site – 205" model to determine the half-maximal inhibitory concentration (IC_{50}).

Fluorescence microscopy

A fresh spore solution at 1 x 10^4 sp/mL was prepared in a 25% PDB medium as reported in the Biological material section and 200 μL were distributed in several microplate wells. Spores were supplemented with SYTOX Green (final concentration of 30 μM) prior to shaking and incubation for 24 hours. Young mycelia of *B. cinerea* were treated by addition of ETD151 at final concentrations of 0.78 and 3.12 μM before a new incubation period of 24 hours. Morphological changes were monitored in transmitted light (TransLight50, 30 ms exposure) with an ImageXpress Micro XL fully automated inverted microscope (Molecular Devices, San Jose, CA, USA) equipped with a Plan Fluor ELWD 40x objective (Nikon). SYTOX Green fluorescence was observed with a Green Fluorescent Protein filter (excitation wavelength, 472 nm; emission wavelength, 520 nm; 100 ms exposure).

Sample preparation for proteomic studies

In a 96-well plate (TPP product), 135 μL of the fresh suspension at 500 sp/mL in minimum medium was distributed in six rows of 10 wells each. Mycelia were cultivated by maintaining the plate for three days in the growth conditions defined previously. Subsequently, 15 μL of sterile MilliQ water was added to the first row as an untreated control. The five other rows were treated with five different concentrations of ETD151, ranging from 31.2 μM to 1.95 μM. The experimental plate was maintained for 24 hours in the previously described growth conditions

until protein extraction. Each microplate was monitored daily by measuring the absorbance at 630 nm with the ELx808 microplate reader (BioTek).

Protein extraction

For each plate, the fungal material (mycelium) from each of the 60 wells was collected by manual pipetting. For each experimental condition (untreated or treated with different concentrations of ETD151), 10 individual wells of a same row were pooled into a single 1.5 mL Eppendorf tube and maintained on ice until use. The fungal material was pelleted by centrifugation for 4 min at 13,000 rpm and 4°C. The fungal pellet was washed twice by up-and-down pipetting with 1 mL of sterile MilliQ water before adding 1 mL of 70% EtOH. The washed mycelia were stored overnight at -80°C. The fungal material was disrupted using a Mill-Mix 20 system (Domel, Železniki, Slovenia). The mycelia were ground in 2-mL tubes filled with 0.5 mm zirconium oxide beads for 10 min at 30 Hz. After centrifugation for 4 min at 13,000 rpm and 4°C, the pellets were collected and dried under CentriVap vaccum (Labconco, Kansas City, MO, USA). Finally, the proteins were extracted by incubating the dried fungal pellet in the presence of 2 M acetic acid, prepared in 50% ACN, for 4 h at 4°C under gentle shaking. After incubation, the extracts were centrifuged for 4 min at 13,000 rpm and 4°C and the protein supernatants were stored at 4°C until use.

Sample preparation for MALDI mass spectrometry analyses

For MALDI MS analyses, a fresh solution of matrix was prepared by adding, up to saturation, a few mg of 4-HCCA in 1 mL of Biotyper solution (Bruker Daltonics) composed of 50% ACN and 2.5% TFA. The samples to be analyzed (0.5 μL) were spotted and immediately covered with 0.5 μL of the matrix solution on an MTP 96 polished steel MALDI target (Bruker Daltonics).

Calibration of the instrument was performed using PepMix complemented with ProtMix. The sample spots were quickly dried under mild vacuum prior to analysis.

Peptide mass fingerprint of *B. cinerea* mycelium by MALDI-TOF mass spectrometry

Mass spectra from protein supernatants described in the Protein extraction section were acquired on an AutoFlex III Smartbeam instrument (Bruker Daltonics) using the FlexControl 3.4 software (Bruker Daltonics) in positive linear mode. The instrument was set up with the following parameters: 200 Hz laser at a 40% global attenuation offset, 20 kV source voltage 1, 18.5 kV source voltage 2, 9 kV lens voltage, 1.82 kV linear detector voltage, 140 ns of pulsed ion extraction delay and 600 Da detector gating. MALDI MS spectra were recorded at the mass range 600 Da to 18 kDa by summing two sets of 1,000 laser shots. Data were previewed using the FlexAnalysis 3.4 software (Bruker Daltonics) and reprocessed in mMass software[46] (version 5.5.0) Average spectra were generated from three selected biological replicates (from a pool of six), based on their fingerprint similarities and their intensities (maximum arbitrary intensity > 10,000). The average spectra were cropped from 1,500 to 16,000 *m/z*, baseline correction was performed with a relative offset of 100 and a precision of 40, along with a smoothing according to the Savitzky-Golay algorithm (window size 5.0 *m/z* in one cycle). The peaks were automatically picked using a signal-to-noise (S/N) ratio of 2.0, a picking height of 90 and an application of baseline. Finally, the average mass spectra were concomitantly and manually curated to select 100 representative ions.

Sample preparation for bottom-up proteomics

Proteins were digested using the modified procedure reported by Masson and colleagues[47]. Briefly, the protein supernatants were dried under vacuum (Labconco), and then suspended with gentle shaking in an ammonium bicarbonate (ABC) buffer (50 mM, pH 7.5) supplemented with 0.1% *Rapi*Gest surfactant. The proteins were reduced with 280 mM dithiothreitol in ABC buffer for 30 min at 56°C in the dark prior to alkylation with 480 mM iodoacetamide in ABC buffer for 30 min at room temperature in the dark. Digestions were carried out for 1 h at 37°C by adding 0.5 μg of trypsin (0.1 μg/μL in ABC buffer). Following this initial digestion, 0.5 μg of trypsin was added before overnight incubation at 37°C. To stop proteolysis and cleave the *Rapi*Gest surfactant, samples were acidified with 8 μL of a 10% TFA and 20% ACN solution and incubated for 30 min at 37°C. Finally, samples were centrifuged for 10 min at 13,000 rpm at room temperature. The digests were transferred into injection vials (Agilent Technology, France) containing 5 μL of 2% ACN acidified with a solution of 0.1% TFA.

Proteomic analyses by nano-LC-ESI-MS/MS

Nano-LC-ESI-MS/MS instrumentation, software, chromatographic columns and other items were obtained from Thermo Fisher Scientific. Peptides were analyzed using an Ultimate 3000 nanoflow HPLC system coupled to a Q-Exactive Orbitrap high-resolution mass spectrometer, controlled by Xcalibur 2.2, Chromeleon Xpress 6.80 and Thermo QExactive Tune 2.5 software. Nano-LC separations were performed according to Pisani and colleagues[48]. Briefly, the digests were loaded at a flow rate of 10 μL/min for 6 min onto a PepMap 100 C_{18} precolumn (300 μm x 5 mm, 5 μm) and separated at a flow rate of 300 nL/min onto an Acclaim PepMap 100 C_{18} nanoviper column (75 μm × 250 mm, 3 μm) maintained at 35°C. Peptides were eluted using a multi-step linear gradient from 2% to 32% and from 32% to 65% ACN in 0.1% (v/v) formic acid

for 94 min and 5 min, respectively. For MS analyses, the mass spectrometer was operating in positive mode and data-dependent acquisition. The instrument acquired a full-range MS scan from 380 to 2000 *m/z* (70,000 resolution, AGC target 3.10^6, maximum IT 200 ms) and then fragmented the top ten peptide ions in each cycle (17,500 resolution, AGC target 2.10^5, maximum IT 100 ms, intensity threshold 4.10^4, excluding charge-unassigned ions, Normalized Collision Energy 27). Parent ions were then excluded from MS/MS for the next 15 s.

Databases searching and annotation

All MS and MS/MS spectral data were analyzed using Proteome Discoverer software (version 2.2.0.388, Thermo Fisher Scientific). Processing and consensus workflows were adapted from manufacturer's basic settings. The acquired MS/MS spectra were matched using the SEQUEST HT[49] search algorithm (University of Washington) against the EnsemblFungi[50] *Botrytis cinerea* B05.10 protein sequence database (http://fungi.ensembl.org/Botrytis_cinerea). The release 42 downloaded on February 16, 2019 contains 13,749 entries. The spectrum identification considered the following parameters: trypsin as proteolytic enzyme with a maximum of two missed cleavages, 6 and 144 amino acids as minimum and maximum peptide lengths, and a tolerance of 10 ppm/0.02 Da for precursor and fragment masses, respectively. Cysteine carbamidomethylation was defined as a static modification. Methionine/tryptophan oxidation, serine/threonine/tyrosine phosphorylation and C-terminal amidation were defined as dynamic modifications. False discovery rates (FDRs), referred to as q-values, and posterior error probabilities (PEPs) for peptide spectral matches (PSMs) were calculated and filtered in the Percolator node using a decoy database[51,52]. Peptides and identified proteins were respectively validated based on high-confidence (FDR < 1%) and medium-confidence criteria (FDR < 5%).

Protein grouping was applied to regroup protein candidates covered by the same set or subset of identified peptides under a representative 'master' protein. Annotations were implemented through Proteome Discoverer using Gene Ontology (biological process, molecular function, cellular compartment), protein families from Pfam and biochemical pathway maps from the Kyoto Encyclopedia of Genes and Genomes (KEGG).

Protein quantification and functional analysis

Label-free quantification was performed using the Proteome Discoverer software. Chromatographic alignment for LC/MS mapping features, created by the Minora Feature Detector for each individual file, was achieved with a maximum retention time shift of 10 min and a mass tolerance of 10 ppm. Protein abundance was determined on intensity of precursor ions of unique and razor peptides.

Activity of complex I/ III and II/III of the respiratory transport chain

Mitochondrial preparation

Two liters of fresh spores of *B. cinerea* were cultured in glucose yeast mycological peptone medium and incubated in Erlenmeyer flasks with stirring for 72h at 22°C. Mycelia were filtered through a 200 μm nylon cloth NITEX (Sefar AG, Heiden, Switzerland), before washing with MilliQ ice water, spinning and weighing. The following steps were performed in a cold room (4°C) to preserve functionality of mitochondria. Mycelia were resuspended in a 0.5 M sucrose/1 mM EDTA/0.3% BSA/20 mM MOPS wash buffer adjusted to pH 7.4. After addition of 5 mM cysteine, the mixture was ground with 1 mm glass beads for three cycles of 30 s with 1 min pauses to cool down the suspension. Fungal material was filtered on a 100 μm nylon cloth

(Sefar) and beads were rinsed with the washing buffer, prior to centrifugation of the filtrate for 10 min at 1,500 g. The supernatant was filtered on a 150 μm nylon cloth (Sefar) prior to centrifugation for 20 min at 15,000 g. The mitochondrial pellet was resuspended in the wash buffer and fractionated in 2-mL aliquots prior to purification on a 1.8 M/1.2 M sucrose gradient, involving centrifugation for 45 min at 36,000 g followed by slow deceleration. Purified mitochondrial fractions at the sucrose bilayer interface were diluted in the wash buffer and centrifuged for 15 min at 36,000 g. Pellets were combined prior to a new washing step to obtain a single purified fraction of mitochondria.

Measurement of inhibition of complex I/III and II/III by colorimetry

The activity of a molecule as a possible electron transport chain complex inhibitor was measured by a potassium ferricyanide-based colorimetric test[53] in the presence of α-ketoglutarate and succinate, substrates of complexes I and II, respectively. Viability of fresh mitochondria was evaluated in 96-well microplates (Greiner Bio One). For complex I, 3 µL of the purified fraction was diluted in 400 μL of Mix I solution (Supplementary data S1) before depositing 88 µL of this mixture into 4 control wells and adding the 0.05 M α-ketoglutarate substrate. After a 3-min incubation at room temperature, the absorbance was measured for 5 min at 405 nm (SpectraMax Plus 384, Molecular Devices). Data was converted to a slope using a linear regression model. Complex II activity was evaluated in the same way using Mix II (Supplementary data S1) and the appropriate substrate. For this assay, the ETD151 peptide diluted in sterile Milli-Q water was compared to two standard inhibitors diluted in DMSO: antimycin A and boscalid. From a dilution range (factor of 3.5) prepared upstream, 2 μL of the molecule to test (50X) was deposited in a well containing 88 μL of fresh mitochondria in Mix I or Mix II, for complex I or complex II, respectively. Immediately for complex I or after 7 min of incubation for complex II,

329 10 µL of 0.05 M substrate were added before incubation for 3 min at room temperature. After a
330 brief stirring, the mitochondrial activity was measured as previously described.
331

RESULTS AND DISCUSSION

Fungal growth inhibition and morphological changes in *Botrytis cinerea*

Several antifungal defensins from insects, like heliomicin[23] and drosomycin[15], or from plants, such as RsAFP2[54] and VvAMP2[55], have been reported to be active against *Botrytis cinerea* at a micromolar range. We have previously shown that ETD151 exhibits a broad-spectrum of activities against several yeasts and filamentous fungi[22] at the micromolar range. However, ETD151 had not been tested on *B. cinerea*. In this study, the antifungal activity of ETD151 was assessed *in vitro* against three-day-old mycelia of *B. cinerea* prepared from a fresh spore solution. In our experimental conditions, growth inhibition reaches a maximum, 78% as measured by optical density, at 6.25 μM of ETD151 (Figure 1A). Based on this value, the half-maximal inhibitory concentration (IC_{50}) was estimated to be 0.59 μM.

The antifungal action of ETD151was monitored by optical microscopy (Figure 1B). At 0.78 and 3.12 μM, ETD151 is able to promote lysis and the release of intracellular content at some points of the growing mycelium, preferentially at the apical end of the hyphae (Fig. 1B, b-c). Such a leakage of cytosolic material suggests a loss of the cell wall integrity. An equivalent observation has already been reported for heliomicin and drosomycin on *B. cinerea* spores, but for these molecules, comparatively weaker effectiveness against the mycelium was recorded[23]. Thus, our data confirm the enhanced activity of ETD151 compared to heliomicin, the reference molecule.

The permeabilization of the fungal membrane has emerged as a trend in the antifungal mode of action of plant defensins[32,56]. The results obtained on *B. cinerea* mycelia treated with the insect defensin homologue ETD151 suggest a similar mode of action. Nevertheless, it remains unclear if ETD151 is internalized or if it remains outside the fungal cells. To assess whether ETD151 is

able to disturb membrane integrity/permeability, the SYTOX Green nucleic acid stain, a cell-impermeant fluorophore, was used. Compared to the control experiment (Fig. 1B, g), in the presence of ETD151, the dye penetrated locally the hyphae and emitted a green-fluorescent signal revealing a compromised plasma membrane (Fig. 1B, h-i).

In addition, ETD151 reduced hyphal elongation with a concomitant disorder in hyphal branching at both tested concentrations (Fig. 1B, e and f, respectively 0.78 and 3.12 μM). Development of the *B. cinerea* mycelium post-treatment highlights the fungistatic aspect of ETD151 activity and may explain the inhibition plateau observed with the fungal growth curve (Fig. 1A). Swelling of hyphae was also noticed with a particularly strong phenotype at 3.12μM (Fig. 1B, f). These morphological changes defined ETD151 as a morphogenic defensin of *B. cinerea*. This is homologous to observations reported for several plant defensins (RsAFP2, HsAFP1, MsDef1) in filamentous fungi[57–59] and confirms commonalities with the antifungal action of the insect defensins. Results obtained after this first series of analyses showed that there are perturbations of the mycelium physiology and morphology, as the optical microscopy pictures and the uptake of the SYTOX Green nucleic acid stain differed between all treatment conditions.

Thevissen and colleagues[28] demonstrated through an ELISA-based assay with *Pichia pastoris* that heliomicin and RsAFP2 interact with fungal membrane lipids called glucosylceramides. All of our structural and biological data support a common mechanism of action for these three defensins, and lead us to suggest that ETD151 interacts with the same fungal partners.

To study the antifungal effects of ETD151 on the intracellular protein content, we used a proteomics study based on a two-step MS workflow, and conducted on *B. cinerea* mycelial extracts. Firstly, a comparison of mass spectrometry (MS) molecular mass fingerprints was conducted by MALDI-MS. This first step was designed to follow the evolution of the peptide

protein profiles within the mass range of 600 Da to 18 kDa. Secondly, a bottom-up proteomics analysis by nano-LC-ESI-MS/MS was performed to identify and characterize the proteins changes. The concentration range from 0.19 to 3.12 μM, which includes the IC_{50} and covers the entire inhibition profile of ETD151, was adopted for a dose-response approach.

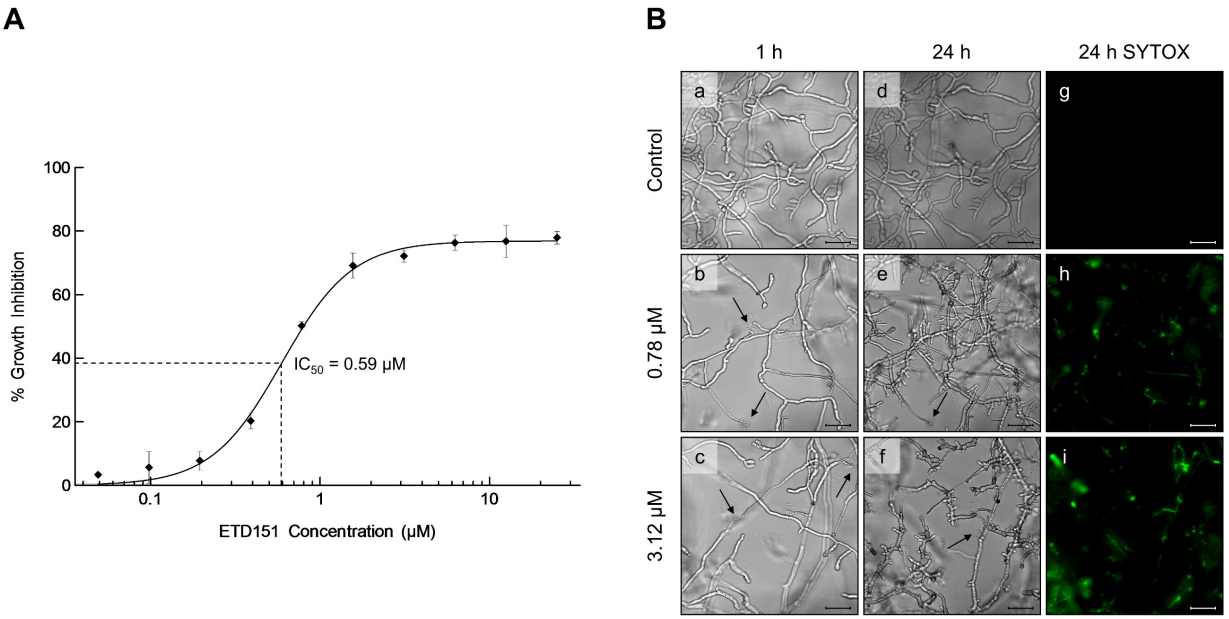

382

383 **Figure 1: Growth inhibition and morphogenic alterations induced by ETD151 in *B. cinerea***

384 (A) Growth inhibition (%) was evaluated on *B. cinerea* three-day-old mycelia produced from
385 fresh spores incubated in modified Tanaka. The dose-response curve was determined by
386 incubating mycelia with ETD151 concentrations ranging from 0.049 to 25 μM (final
387 concentration in $\log_{10}$) for four days. The dotted lines indicate the IC_{50}. Data are the means of
388 triplicate measurements. Error bars denote standard deviation. (B) Morphogenic alterations of *B.*
389 *cinerea* mycelia obtained from a fresh culture of spores were observed microscopically after one
390 hour (a, b, c) and 24 h (d, e, f) of incubation in Potato Dextrose Broth diluted by 1/4th. Mycelia
391 were incubated in the absence (control experiment, a, d) or the presence of ETD151 at a final
392 concentration of 0.78 μM (b, e) and 3.12 μM (c, f). SYTOX Green signal was measured by
393 fluorescence microscopy 24 h post-treatment (h, i) on the same experimental plate wells as the
394 control experiment (g). Arrows indicate lysis of hyphae. Scale bar = 50 μm.

Protocol development to prepare *B. cinerea* mycelial extracts

Fungal culture, extraction and MALDI-MS analysis protocols have been developed for this study. The extraction protocol is inspired by the work of Schulthess and colleagues[60], using 35% formic acid for the BioTyping of clinical molds. The objective was to establish the optimal parameters for recording the most representative MALDI peptide signatures/molecular mass fingerprints (MFPs) of *B. cinerea*, with or without different concentrations of ETD151. The following parameters were reviewed: the starting concentration of *B. cinerea* spores, the mycelial culture duration in microplate, the treatment duration with ETD151 and the extraction process to generate mycelial extracts. The development of the protocols was focused on the conditions providing the most reproductible MFPs and with a rich molecular diversity. We settled on a starting concentration of 500 sp/mL prior to three days of growth in microplate and a 24h-treatment of the mycelia with ETD151. Peptides/proteins were extracted by grounding the mycelia with zirconium oxide beads, drying the pellet and incubating it in the presence of 2 M acetic acid solution prepared in 50% ACN (personal communication, Victor Masson and Philippe Bulet). The different parameters for MALDI-MS analysis were optimized for an optimal detection (in terms of sensitivity, resolution, reproducibility and accuracy) of molecular ions between 1,500 – 12,000 mass *m/z* of the *B. cinerea* mycelial extracts.

Peptide mass fingerprint of *B. cinerea* mycelium in response to ETD151

Once the experimental methodology had been established, MALDI-MS analyses were performed directly on *B. cinerea* mycelial peptide/protein extracts, and restricted to peptides and small proteins (<20 kDa) as a preliminary approach to assess the antifungal effect of ETD151 at the molecular scale. Three-day-old mycelia were incubated for 24 h with the defensin following

418 the previous concentration range, from 0.19 to 3.12 μM final concentrations. Average spectra
419 (n=3) were generated from biological replicates to first, highlight modifications of the
420 peptide/protein composition in the presence of ETD151 and second, visualize a putative dose-
421 response effect (Figure 2). For each concentration, a manual selection from automatic peak
422 labeling resulted in a representative peak list of 100 ions. Similarities between MALDI MFPs
423 were calculated following the conservation of representative ions (Supplementary data S2).

424 In the presence of 0.19 μM of ETD151, no strict molecular change was observed on the MFPs.
425 Compared to the untreated mycelia, MFPs were very similar with 91% identity (Fig. 2A). This
426 observation is consistent with the very reduced growth inhibition effect (less than 10%) observed
427 at this dose (Fig. 1A). From 0.39 μM of ETD151, the antifungal activity of ETD151 has a
428 significant impact on the MFPs recorded. Several modifications were highlighted on the MFPs
429 compared to untreated mycelia, with identity dropping to 68% (Fig. 2B). Differences in the
430 peptide/protein profiles are significant in particular within the 6,000-9,000-mass range
431 (Supplementary data S3). At 0.39 μM, two sets of peptides/proteins within the 9,000-10,000 and
432 14,000-17,000 mass ranges emerged; those were not detectable in the control MFP or at an
433 ETD151 concentration of 0.19 μM.

434 At 0.39 μM or higher doses of ETD151, the MALDI-MS spectra showed similar overall MFPs
435 (Fig. 2C). Indeed, the dose of 0.39 μM shares 92%, 84% and 77% identity with the 0.78, 1.56
436 and 3.12 μM doses, respectively. Several ions within the 9,000-10,000 and 14,000-17,000 mass
437 ranges display intensity variation according to the concentration of the defensin with intensities
438 increasing as the concentration reaches 0.39 μM (Supplementary data S2). These results suggest
439 that MALDI-MS could be a rapid and simple method to assess the impact of an antifungal
440 molecule on its fungal target. The modifications of the MFPs observed between the proteins

441 extracted from the control experiment versus *B. cinerea* mycelia treated with different doses of
442 ETD151 also revealed that ETD151 modified the peptide/protein profiles of *B. cinerea* mycelia,
443 in a dose dependent manner up to a concentration that is more than the IC_{50} (0.59 μM).

444 Despite the extraction method used, including removal of the culture supernatant and two
445 successive washing steps of the mycelia, the ion observed at *m/z* 4,839 corresponds to ETD151.
446 It is worth mentioning that the intensity of this ion does not decrease with two additional washes
447 (unpublished data). This suggests that in our experimental conditions, ETD151 was interacting
448 with the membrane of the altered mycelium of *B. cinerea*, or was entering the mycelium. Note
449 that the arbitrary intensity (a.i.) of the ETD151 ion increases with the concentration of ETD151
450 used, from $1.9.10^3$ a.i. at 0.19 μM to 174.103 a.i. at 3.12 μM (Supplementary data S2).

451 As important modifications of the MFPs are observed within the highest molecular mass range
452 detectable in our MALDI-MS conditions, this preliminary approach attests to the antifungal
453 effect of ETD151 on *B. cinerea* and prompted us to analyze the mycelial extract of *B. cinerea*
454 treated with ETD151 at the peptide/protein scale using a bottom-up proteomics approach.

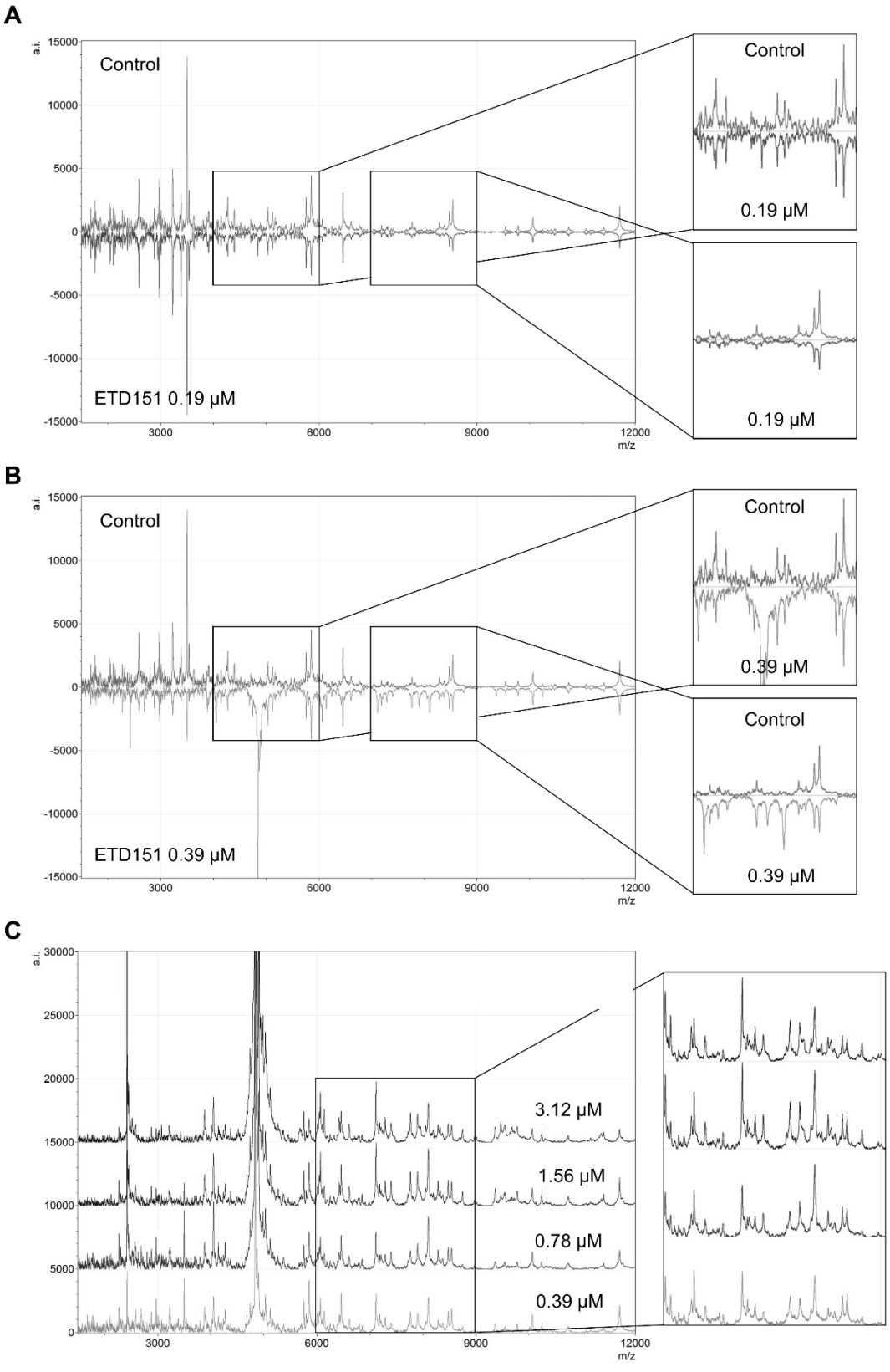

Figure 2: MALDI profiling of extracts of *B. cinerea* mycelia treated with ETD151

457 The MALDI mass spectra show the average MALDI-molecular mass fingerprint (n=3) from
458 mycelial protein extracts treated or not with the antifungal peptide ETD151. The mass spectra
459 are recorded in the 1,500 – 12,000 mass (*m/z)* range, for untreated mycelia (Control) *versus*
460 mycelia treated with 0.19 μM ETD151 (A) and 0.39 μM ETD151 (B). Zooms show enlarged
461 area at the 4,000-6,000 and 7,000-9,000 mass ranges. The mass spectra recorded when the
462 mycelial cultures were treated with 0.39, 0.78, 1.56 and 3.12 μM ETD151 are also reported (C).
463 The zoom shows the enlarged mass range (*m/z*) between 6,000 and 9,000.

Effect of ETD151 on *B. cinerea* mycelium by bottom-up proteomics

Differential proteomics analysis in response to ETD151

Our MALDI-MS results showed that the MFPs of the mycelial preparations are altered in response to the different concentrations of ETD151 used to treat *B. cinerea* mycelia. To have a better picture of the molecular response of *B. cinerea* mycelium upon our ETD151 treatment, we used gel- and detergent-free proteomics to monitor protein changes on mycelial extracts. *B. cinerea* mycelial peptide/protein acidic extracts prepared for MALDI-MS were dried under vacuum prior to reduction-alkylation-enzymatic digestion. *B. cinerea* protein digests were then analyzed by LC-ESI-MS/MS analysis as a conventional bottom-up proteomics approach. To evaluate the methodology implemented and validate our data analysis strategy, two sets of experiments were performed (Figure 3) allowing to generate two datasets (I and II). First, three individual cultures were harvested, following the same experimental procedure, from the collection of non-treated or treated cultures with different doses of ETD151 (Fig. 3A, dataset I). Second, a triplicate experiment was conducted on three individual plates with three-day-old mycelia (Fig. 3B, dataset II) originating from a unique culture of spores.

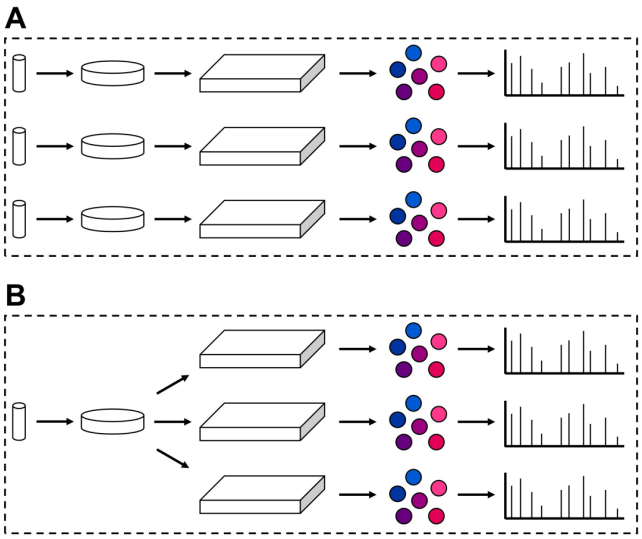

Figure 3: Workflow developed for the bottom-up proteomics approach on *B. cinerea*

Fresh fungal material was obtained from a calibrated stock solution of *B. cinerea* spores cultivated for seven days on a PDA medium. A fresh spore suspension was prepared and distributed in a 96-well plate prior to incubation. Three-day-old mycelia were treated with water (control experiment, blue) or with different concentrations of ETD151: 0.19 μM (light blue), 0.39 μM (light pink), 0.78 μM (pink), 1.56 μM (light purple) and 3.12 μM (purple). After a 24h-incubation, mycelia were collected and proteins were extracted. Samples were prepared for bottom-up proteomics and digests analyzed by LC-ESI-MS/MS prior to data processing. (A) The dataset I groups three individual cultures, while dataset II (B) is a triplicate experiment corresponding to three individual plates coming from a unique culture of spores.

Dataset I allowed the identification of 1,431 typical proteins with molecular masses ranging from 4.8 to 466 kDa. Among these proteins, 1,430 originate from *B. cinerea* while the last one corresponds to ETD151, detected by LC-ESI-MS/MS with 80% coverage (see raw data). We observed an increase in the number of identified proteins in response to increasing concentrations of ETD151 (Figure 4A, diamond plots). The average number (Fig. 4A, black diamonds) of identified proteins was 532 and 534 for control and 0.19 μM ETD151, respectively. This average number increased to 794 and 899 proteins when the cultures were treated with 0.39 and 3.12 μM ETD151, respectively. The increase in the number of proteins extracted in response to elevated concentrations of ETD151, may reflect a perturbation of the integrity of the cell membrane of the mycelium and/or the stimulation of the expressions of series of genes, and would corroborate microscopic data (see Fig. 1B) that points to an antifungal effect of the defensin on *B. cinerea*. The reproducibility within dataset I was assessed for each concentration of ETD151 as the average ratio between the number of identified proteins in each experiment and the number of recurrent proteins (Fig. 4A, histograms), as identified in all three experiments. The reproducibility within the control experiment and after a treatment with 0.19 μM ETD151was at 68 ± 11 % and 67 ± 8 % , respectively. For 0.39 μM ETD151, it was 73 ± 6 %, and for higher concentrations of ETD151, the reproducibility was 75 % with a standard deviation ≤ 6 % (Fig. 4A, square plots). Furthermore, a principal component analysis (PCA) was run on proteins of dataset I and showed a clustering of experiments according to the concentration of ETD151 (Figure 4B). Control and 0.19 μM samples were clearly separated from the other tested concentrations by the first component (42.8%). The first component (PC1, Fig. 4B) may reflect the molecular impact of ETD151 on the *B. cinerea* mycelium. Samples from 0.39 to 3.12 μM of ETD151 could not be separated according to the second component (13.4%).

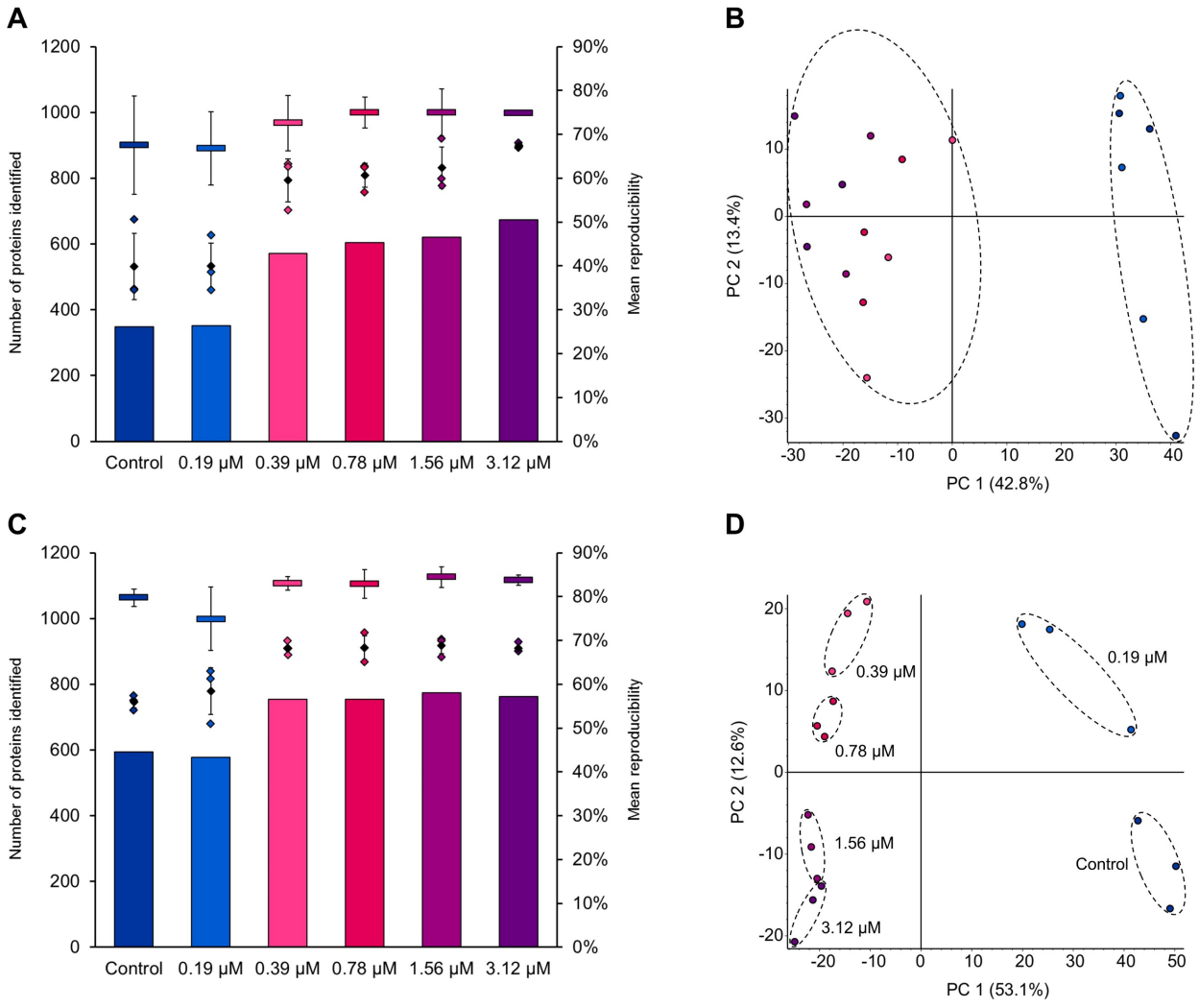

Figure 4: Protein identification of *B. cinerea* mycelial extracts and assessment of reproducibility

(A) The number of proteins identified in samples of dataset I is shown according to the concentration of ETD151. Replicates and mean, along with the standard deviation, are represented by colored and black diamond-shape plots, respectively. Histograms indicate the number of recurrent proteins between all three replicates, the basis for calculation of reproducibility. Mean reproducibility is represented by colored rectangles, along with the standard deviation. (B) The Principal Component Analysis generated by Proteome Discoverer is

shown for the 1,431 proteins identified within dataset I. Experiments are visualized according to the concentration of ETD151 and the color code introduced previously. (C) The number of proteins identified in samples of dataset II is reported according to the concentration of ETD151. Values are represented in the same way as dataset I, and data of the Principal Component Analysis generated for the 1,468 proteins identified in dataset II are shown in (D).

Dataset II, a triplicate of three individual plates, identified 1,468 master proteins from a 4.8 to 466 kDa mass range. The goal of this experimental design was to estimate the impact of the initial culture of spores or of the harvest method on the reproducibility of the data. It should be noted that working simultaneously on three individual microplates significantly complexified the experimental protocol. Treatment of mycelia with ETD151, as well as the manual collection of samples from each microplate, should be completed within a very short period of time. As reported previously for dataset I, the average number of identified proteins increased upon treatment with ETD151 (Figure 4C). As with dataset I, we observed an increase in the number of identified proteins in response to increasing concentrations of ETD151 (Fig. 4C, diamond plots). The average numbers (Fig. 4C, black diamonds) of identified proteins were 745 and 778 for the control and 0.19 μM ETD151 samples, respectively. This average number increased to 910 and 917 proteins when the cultures were treated with 0.39 and 3.12 μM ETD151 (Fig. 4C, diamond plots). The reproducibility was assessed in the same way as for dataset I (Fig. 4C, histograms). In the control and 0.19 μM samples, the reproducibility was 80 ± 2 % and 75 ± 7 %, respectively. For higher concentrations of ETD151, the reproducibility ranged from 83 to 84 % with a standard deviation ≤ 3 %. PCA was also run on dataset II (Figure 4D). As observed for dataset I, the first component (53.1 %) separated Control and 0.19 μM samples from the other concentrations. Unlike the PCA on dataset I, the second component (12.6 %) allowed to separate the different samples according to the concentrations of ETD151.

This new experimental design improved the robustness of the data as the average reproducibility between dataset I and II increased by 9% while the variability between replicates decreased, as reflected by the reduction in standard deviations. This explains the greater weight in our PCA analyses of the first component, at 43% and 53% in datasets I and II, respectively.

550 Interestingly, in terms of the average number of identified or recurrent proteins, the samples
551 treated with 0.19 μM ETD151 showed values closer to the control experiments (see above),
552 which is supported by the clustering observed for control and 0.19 μM ETD151 replicates on one
553 side within the first component in PCA whereas replicates for higher concentrations aggregated
554 on the other side. Although the results improved in dataset II, samples for 0.19 μM ETD151
555 were the only ones with a reproducibility below 80% and a standard deviation > 5%. This
556 concentration of ETD151 appeared as an inflection point in the molecular effect of the antifungal
557 peptide as the changes induced by ETD151 barely allow to distinguish control from 0.19 μM
558 samples. Finally, datasets I and II were grouped to consolidate data analysis. Indeed, both dataset
559 shared similar properties on the increase in identified and recurring proteins for identical
560 concentrations of ETD151, from 0.39 to 3.12 μM.
561 The protein distributions were represented on a multidimensional Venn diagram based on six-
562 experimental datasets (untreated *vs* treated with five increasing concentrations of ETD151)
563 (Figure 5). The Venn diagram is a simplified tool, free of statistical test, allowing to classify
564 proteins from large datasets and to highlight groups of interest in our study. The diagram we
565 obtained, allowed to represent the logical relations between the 1,592 summed proteins identified
566 in the two datasets I and II. Among these proteins, 42 were specifically found in the non-treated
567 samples and 21 to 26 of them specifically in each concentration of ETD151 (21 in 0.19 μM, 22
568 in 0.39 μM, 24 in 0.78 μM and 26 in 1.56 μM). We found the most abundant number of specific
569 proteins (44) when the mycelial culture was treated at 3.12 μM, the highest concentration of
570 ETD151. Interestingly, as previously discussed, at the inflexion point, 82 proteins were found
571 mutually in the control experiments and in samples treated with 0.19 μM ETD151. Overall, 676
572 proteins were observed to be common to all samples, 120 proteins were found in all treated

573 samples, regardless of the concentration of ETD151, and 185 proteins were specifically found at
574 the concentrations of 0.39 μM ETD151 and above.

575 Our results demonstrated that ETD151 affected the molecular composition of *B. cinerea*
576 mycelial samples and confirmed, over a wide mass range (4.8 – 466 kDa), the results presented
577 previously by MALDI-MS MFPs up to 18 kDa. This comparative approach allows us to build an
578 overview of the behavior of protein groups following treatment with the peptide and to select by
579 label-free quantification characteristic proteins and metabolic pathways altered upon treatment
580 with ETD151.

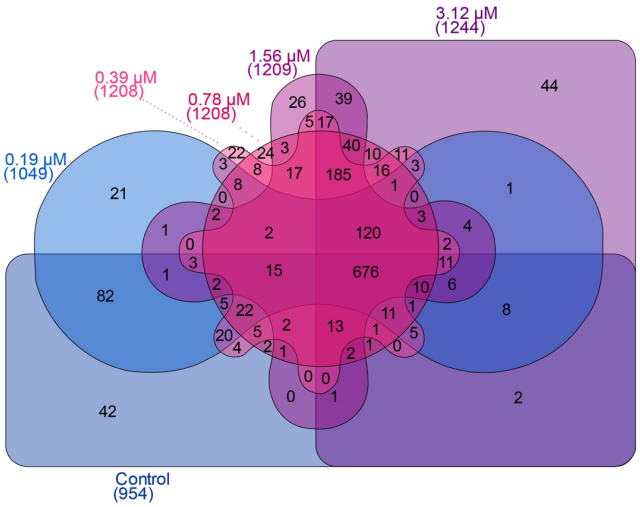

Figure 5: Multidimensional six-set Venn diagram

The Venn diagram generated on www.interactivenn.net displays the 1,592 summed proteins from datasets I and II according to their presence or absence in mycelia treated with increasing concentrations of ETD151 : 0.19 μM (light blue), 0.39 μM (light pink), 0.78 μM (pink), 1.56 μM (light purple) and 3.12 μM (purple).

587 Label-free quantification analysis

588 We identified 1,592 proteins and among them, 1,559 were quantified according to a label-free
589 approach. Abundance ratios and p-values were not calculated for 33 proteins. Significantly
590 dysregulated proteins were selected with volcano plots according to a p-value equal to 0.95 and a
591 ± 2-fold change (Supplementary data S4). Volcano plots are commonly used to display the
592 results of -omics experiments. This methodology allowed to highlight differentially abundant
593 proteins in the presence of different concentrations of ETD151 (Figure 6A). Increasing
594 concentrations of ETD151 of 0.19, 0.39, 0.78, 1.56 and 3.12 μM resulted in the downregulation
595 of 23, 56, 66, 73 and 85 proteins, respectively (light grey); and in the upregulation of 86, 173,
596 162, 158 and 162 proteins, respectively (dark grey). Statistical analysis determined that out of the
597 340 proteins identified, 134 were significantly downregulated, and 204 were significantly
598 upregulated (Figure 6B). Two proteins (Bcin02p06900, 40S ribosomal protein S20e, and
599 Bcin12p02600, putative mitochondrial protein), were downregulated in the presence of 0.19 μM
600 of ETD151 and upregulated at higher concentrations.

601

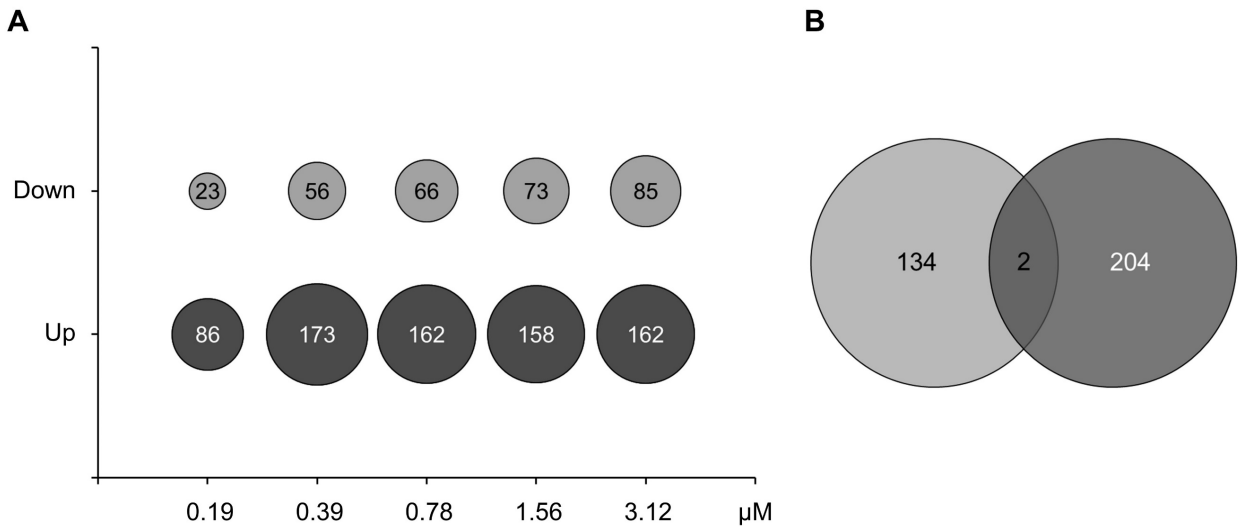

602

603 **Figure 6: Significantly dysregulated proteins upon treatment of *B. cinerea* mycelium with**

604 **ETD151**

605 (A) Bubble chart summarizes the differentially abundant proteins with a ± 2-fold change and a P-

606 value ≤ 0.05 as detailed in volcano plots (see Supplementary data S4). (B) The Venn diagram

607 pooling the two sets of proteins modulated upon treatment with ETD151. A total of 340 unique

608 proteins are reported including 134 downregulated (light grey), 204 upregulated (dark grey) and

609 two that were both down- and upregulated (intersecting of the two sets).

610

Gene ontology and network analysis

Proteins were annotated using ProteinCenter (Proteome Discoverer) to investigate molecular functions, biological processes, and cellular components from the Gene Ontology (GO) database (Figure 7). The molecular function-based categorization showed that among the 340 selected proteins, 168 (42%) could not be classified while the others were classified according to the GO terms as follow: 103 (26%) have catalytic activities (GO:0003824), 92 (23%) have binding properties (GO:0005488), 27 (7%) contribute to the structural integrity of a complex or its assembly within or outside a cell (GO:0005198), 7 (2%) act as transporters (e.g. lipids, proteins, oxygen) (GO:0005215), 4 (1%) are regulators of molecular functions (GO:0098772), and finally 2 (0.5%) were recognized as having antioxidant activity (GO:0016209) (Fig. 7A). Following the biological process-based categorization, 178 (49%) among the 340 proteins could not be classified. The most affected process is metabolism with 125 proteins (34%) (GO:0008152). The rest of the proteins are involved in biological processes such as (i) localization (21, 6%) (GO:0051179), (ii) regulation (15, 4%) (GO:0065007), (iii) cellular component organization (14, 4%) (GO:0071840), (iv) response to a stimulus (7, 2%) (GO:0050896), or (v) cellular process (2, 1%) (GO:0009987) (Fig. 7B). Cellular component annotation was also investigated despite a lack of information for *B. cinerea* in this GO categorization. Among the 340 selected proteins, 288 (84%) could not be classified (data not shown).

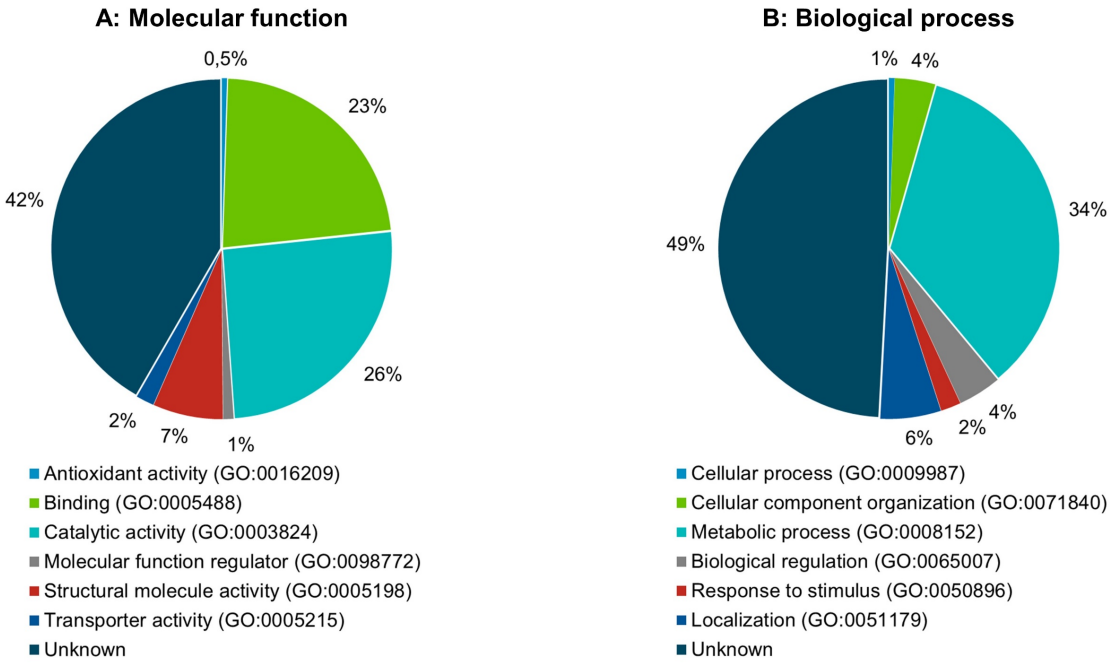

Figure 7: Gene Ontology of dysregulated proteins in *B. cinerea* mycelial extracts

Proteins selected (340) according to their differential abundance are categorized according to their (A) molecular function and (B) role in biological processes.

Molecular impact of ETD151 on *B. cinerea* pathways

Significantly modulated proteins upon treatment with ETD151 were searched in *Botrytis cinerea* KEGG pathways (117 pathways reported). From the 339 proteins (340 minus ETD151) previously selected, 106 were successfully mapped over 67 different pathways with a varied number of hits, from 1 to 38 matched proteins per map (Supplementary data S5). Pathways with less than five hits were not considered for further investigations, as a low number of matched proteins did not allow us to interpret their relevance in the mechanism of action of ETD151 on *B. cinerea*. Moreover, most of these maps were included in carbohydrate, lipid or amino acid metabolisms. Direct effects on these pathways had been evaluated by measuring the uptake and incorporation of radiolabeled precursors (^{14}C-glucose, ^{3}H-phenylalaline and ^{14}C-acetate) by *Botrytis cinerea* spores in the presence of ETD151 (data not shown). ETD151 did not interfere with carbohydrate, protein and lipid biosynthesis confirming that modulated proteins in previously mentioned pathways resulted from global stress in response to an antifungal molecule. The following global pathway maps (metabolic pathways (bfu01100), biosynthesis of secondary metabolites (bfu1110), biosynthesis of antibiotics (bfu01130) and carbon metabolism (bfu01200) were also excluded from the analysis in favor of the study of specific maps. By considering the filters previously described, six pathways were impacted by the treatment, namely ribosome (bfu03010), spliceosome (bfu03040), protein processing in endoplasmic reticulum (bfu04141), endocytosis (bfu04144), MAPK signaling pathway (bfu04011), and oxidative phosphorylation (bfu00190).

655 Effect on ribosomes

656 Ribosomes are essentially very complicated nano-factories for producing proteins. In our
657 study, 80 proteins, out of a total of 103 reported in this pathway for *B. cinerea*, were identified in
658 datasets I and II (Supplementary data S6). Upon treatment with ETD151, 25 ribosomal proteins
659 were significantly modulated. Starting at a concentration of 0.39 μM of ETD151 this included 24
660 up-regulated proteins, as eight in the small subunit 40S: Bcin01p00980/S2e,
661 Bcin02p06900/S20e, Bcin03p05970/S9, Bcin03p06990/S16e, Bcin03p07110/S15Ae,
662 Bcin03p07120/S12e, Bcin07p00830/S13 and Bcin08p00760/S29e, and 16 in the large subunit
663 60S: Bcin01p09660/L35Ae, Bcin03p01900/L39e, Bcin03p06530/L7Ae, Bcin03p07630/L7e,
664 Bcin05p01600/L18Ae, Bcin05p06070/L38e, Bcin07p00520/L27e, Bcin08p03200/L4,
665 Bcin09p03550/L14e, Bcin09p05600/L30e, Bcin10p04290/L17e, Bcin10p04590/L12e,
666 Bcin14p04100/L22e, Bcin08p02490/L32e (starting from 0.19 μM), Bcin14g04790/L15e
667 (starting from 0.19 μM) and Bcin08p00590/L15 (at 0.39 and 0.78 μM). Bcin14p02830, 60S
668 ribosomal protein L3e, is the only downregulated protein, starting from the concentration of
669 ETD151 of 0.39 μM. To our knowledge, there is no report in the literature concerning antifungal
670 insect or plant defensins directly targeting protein biosynthesis in ribosomes. The modulation of
671 ribosome-related subunits might reflect an attempt to keep protein synthesis at optimal levels as
672 the presence of the antifungal defensin ETD151 disturbs protein biosynthesis and degradation.
673
674 Effect on the spliceosome

675 The spliceosome is a dynamic complex, located primarily within the nucleus of eukaryotic
676 cells, and plays an essential role in the maturation process of mRNA. In our study, 27 proteins,
677 out of a total of 84 reported in this pathway for *B. cinerea*, were identified (Supplementary data

678 S6). Upon treatment with ETD151, 7 proteins were significantly dysregulated.
679 Bcin08p03160/Smd2 and Bcin08p06600/Smd3, small nuclear ribonucleoproteins, and
680 Bcin09p07050/Lsm7, an snRNA-associated Sm-like protein, were upregulated at 0.39 μM of
681 ETD151 and higher concentrations. In contrast, four proteins were downregulated in the
682 presence ofETD151: Bcin09p06610/PPIL1 peptidyl-prolyl cis-trans isomerase-like from 0.19
683 μM, Bcin08p00660/Prp1 pre-mRNA-processing factor from 1.56 μM, Bcin09p06940/SF3b
684 splicing factor and Bcin13p05240/THOC THO complex subunit at 3.12 μM. There is no clear
685 tendency to interpret the molecular changes induced by ETD151 on this pathway. Moreover, as
686 there is no report in the antifungal defensin literature of a direct effect on the spliceosome, this
687 pathway was not considered for the continuation of the work on the mechanism of action of
688 ETD151.
689
690 Effect on protein processing in the endoplasmic reticulum (ER)
691 The ER is a continuous membrane system found within the cytoplasm of eukaryotic cells
692 allowing for protein synthesis, folding, modification and in some cases transport to the Golgi
693 apparatus through vesicles. In our study, 37 proteins, out of a total of 70 reported in this pathway
694 for *B. cinerea*, were identified (Supplementary data S6). Upon treatment with ETD151, seven
695 proteins were significantly dysregulated. Bcin13p00700/ERGIC53 and Bcin05p05180/OS9 are
696 upregulated starting a concentration of 0.39 μM. Bcin07p01430/Sec62, Bcin02p05070/Sec24,
697 Bcin01p05490/Bcnpl4 and Bcin10p00510 are downregulated starting at 0.39 μM of ETD151.
698 These proteins play roles in the transport of proteins from the ER. Proteins that are located in the
699 ER and/or Golgi apparatus, are interesting to highlight, as sphingolipids, including
700 glucosylceramides, fungal partners of RsAFP2[61] and possibly ETD151, are synthesized in the ER

and Golgi apparatus[62]. Further investigation will be necessary to monitor a direct effect of ETD151 on glucosylceramide biosynthesis and/or export.

Effect on endocytosis

Endocytosis is a cellular process in which substances (e.g. nutrients, plasma membrane proteins, lipids) are brought into the cell. Interestingly, research on antifungal plant defensins demonstrated that certain ones, such as MtDef4, Psd1 and NaD1, can be internalized by fungal cells upon interaction with a membrane partner[32]. Mechanisms of fungal cell entry are still under investigation, however it is known that MtDef4 and NaD1 internalization are energy dependent and require endocytosis in *Neurospora crassa*[33] and *Candida albicans*[63], respectively. In our study, 35 proteins, out of a total of 58 reported in this pathway for *B. cinerea*, were identified (Supplementary data S6). Upon treatment with ETD151, 7 proteins were significantly dysregulated. Three of them were upregulated in the presence of ETD151: Bcin13p05610/CAPZA capping protein (actin filament) muscle Z-line starting at a concentration of 0.19 μM, Bcin11p01640/VPS26 and Bcin11p01920/VPS35 vacuolar protein sorting-associated protein at a concentration of 0.39 μM. In contrast, four were downregulated: Bcin01p06150/Arp2/3 actin related protein 2/3 complex subunit, at a concentration of 0.19 μM only, Bcin03p0497/Epsin membrane protein and Bcin13p04030/ArfGAP stromal membrane-associated protein starting at the concentration of 0.39 μM, and Bcin13p00990/Hrs hepatocyte growth factor-regulated tyrosine kinase substrate at the concentrations of 0.78 and 1.56 μM. These results could be valuable for future research on the mechanism of action of ETD151, and specifically the behavior of the antifungal defensin upon its interaction with the fungal membrane.

724

725 Effect on MAPK signaling pathway

726 Fungi, like other eukaryotes, rely on the rapid transduction of signals through the mitogen-
727 activated protein kinase (MAPK) pathway in order to overcome environmental stresses such as
728 the addition of chemical fungicides and antifungal peptides. At lower concentrations, one or
729 more stress response pathways are activated to respond to the cell damage. At higher
730 concentrations, the fungal stress response leads to the inhibition of cell growth or induction of
731 cell death. Several antifungal plant defensins[34] (e.g. RsAFP2, Psd1, MsDef1) are known to
732 activate the MAPK pathway, with the cell wall integrity pathway (CWI), inducing changes to
733 cell wall biogenesis, β-glucan synthesis and the organization of the actin cytoskeleton. The
734 Defensin NaD1 activates the high-osmolarity glycerol (HOG) pathway[63], leading to an increase in
735 intracellular glycerol which provides protection against osmotic stress. In our study, 23 proteins,
736 out of a total of 56 reported in the HOG pathway (bfu04011) for *B. cinerea*, were identified in
737 datasets I and II (Supplementary data S6). Upon treatment with ETD151, three proteins were
738 dysregulated in the CWI pathway: Bcin08p03780/Rom1,2 (down at 3.12 μM),
739 Bcin02p06930/Fks2 (up starting from 0.19 μM) and Bcin16p00490 (up starting from 0.19 μM);
740 one protein was dysregulated in the HOG pathway: Bcin16p04710 (down starting from 0.39
741 μM). The protein Bcin16p00490/Cdc28, in both CWI and HOG pathways, was also upregulated
742 starting from 0.19 μM.

743

744 Effect on oxidative phosphorylation

745 Oxidative phosphorylation, coupling the cascade of oxidation-reduction of the mitochondrial
746 respiratory chain and the phosphorylation of ADP to ATP, is an essential metabolic pathway for

747 the survival of most aerobic eukaryotic organisms. In our study, 60 out of a total of 72 reported
748 proteins in the *B. cinerea* bfu00190 pathway were identified (Figure 8A). Upon treatment with
749 ETD151, two subunits of NADH dehydrogenase (complex I) Bcin08p06780/NDUFV1,
750 Bcin08p01490/NDUFA8 were significantly up-regulated starting from a concentration of
751 0.78 μM of ETD151. Similarly, a subunit of succinate dehydrogenase (complex II)
752 Bcin05p04430 was also up-regulated at 0.19 μM of ETD151. By contrast, a subunit of
753 ubiquinol-cytochrome c reductase (complex III) Bcin03p08370/QCR9 was significantly down-
754 regulated at 0.19 μM of ETD151. Finally, several subunits of F-type H+-transporting ATPase
755 (complex V) were significantly modulated upon treatment: Bcin02p02510/epsilon (down at 0.19
756 μM), Bcin10p01500/c (up starting at 0.39 μM), Bcin02p02250/e (down at 3.12 μM) and
757 Bcin12p02610/k (down starting at 1.56 μM). Our proteomics data suggested a mitochondrial
758 dysfunction in the presence of the antifungal defensin ETD151. To go further, the direct activity
759 of ETD151 on complexes I to III of the mitochondrial respiratory chain was assessed and
760 compared to boscalid and antimycin, two molecules providing reference profiles as inhibitors of
761 succinate dehydrogenase and ubiquinol-cytochrome c reductase, respectively (Figure 8B). A
762 colorimetric assay based on the reduction of ferricyanide allowed to measure combined activities
763 of complexes I and III on the one hand, and complexes II and III on the other hand. The activity
764 of boscalid demonstrated a partial inhibition (50%), when testing complexes I and III together,
765 and a total inhibition, when testing complexes II and III together. The activity of antimycin A
766 was characterized by a total inhibition in both associations of complexes. In the presence of
767 ETD151, no inhibition was measured regardless of the tested complex, using up to 50 μM of the
768 antifungal defensin. This result confirmed that ETD151 does not interact directly with complexes
769 of the mitochondrial respiratory chain. Mitochondrial dysfunction highlighted by our proteomics

770 data may result from mitochondrial membrane perturbation, reflecting a secondary effect of
771 ETD151 disturbing cell membrane integrity.

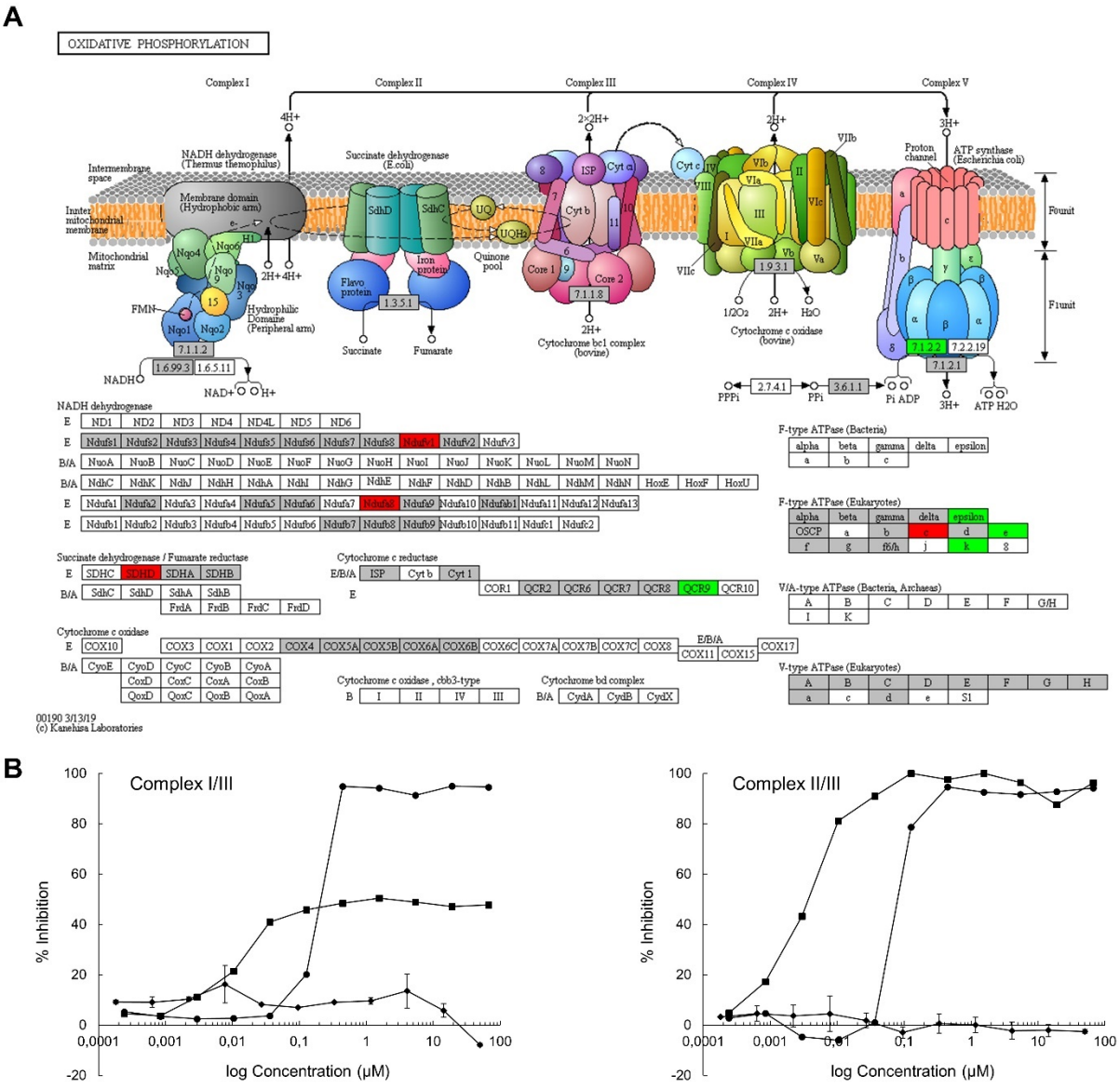

Figure 8: Effect of ETD151 on the *B. cinerea* mitochondrial chain respiration complex

(A) Mapping of dysregulated proteins upon treatment with ETD151 on the oxidative phosphorylation pathway (bfu00190) from the KEGG database. For *B. cinerea*, 72 proteins are reported on this map of which 60 were identified in this study (grey). Eight differentially abundant proteins were found, upregulated (red) and downregulated (green). (B) Activity of ETD151 (diamond), boscalid (square) and antimycin A (circle) on complex I/III and complex

779 II/III of *B. cinerea* mitochondria. Results for ETD151 are expressed as the average of a duplicate

780 experiment along with standard deviation.

Conclusions & Perspectives

Through this study, we demonstrated that the proposed approach offers an experimental workflow to evaluate changes in the peptide and protein contents of mycelial extracts of *B. cinerea* in response to different concentrations of the antifungal peptide ETD151. As an initial approach, molecular mass fingerprinting by MALDI-MS allowed to highlight molecular changes in *B. cinerea* mycelia treated with ETD151. Even with spectra obtained on a partial mass range (<20 kDa), it could be interesting to compare average fingerprints in the presence of ETD151 to spectra generated with other antifungal defensins. This comparison could direct the study on the mechanism of action of ETD151 toward other peptides. As a second step, bottom-up analyses of mycelial extracts provided robust and reproductible data, necessary to study in-depth molecular changes induced by ETD151 on *B. cinerea*. Thus, we revealed six pathways (ribosome (bfu03010), spliceosome (bfu03040), protein processing in endoplasmic reticulum (bfu04141), endocytosis (bfu04144), MAPK signaling pathway (bfu04011), and oxidative phosphorylation (bfu00190)) impacted by the insect defensin. At least for one of these pathways, we also demonstrated that the observed impact must be indirect. Indeed, we clearly demonstrated that there was no direct effect of ETD151 on the *B. cinerea* mitochondrial respiration chain. As a conclusion, proteomics could offer a way to improve the research strategy into the resolution of antifungal mechanisms of action by targeting preferentially involved proteins or metabolic pathways. Finally, an additional objective for a deeper understanding of the mechanisms of action of ETD151 is to study the interaction of ETD151 with lipid components of the fungal membrane, such as e.g. glucosylceramides.

Supporting Information

The following files are available free of charge.

S1: Composition of reaction mix for the activity test on respiratory chain complex

S2: MALDI-MS fingerprinting of *B. cinerea* mycelial extracts

S3: Distribution of MALDI-MS ions in *B. cinerea* mycelium fingerprints

S4: Volcano plots depicting significantly dysregulated *B. cinerea* proteins in the presence of ETD151

S5: List of KEGG *B. cinerea* pathways with significantly dysregulated proteins

S6: Mapping of *B. cinerea* dysregulated proteins on pathways impacted upon treatment with ETD151

Author Contributions

Idea and design of the study: PB, CL, TK.

Mass spectrometric analysis: TA, PB, SV.

Pathway analysis: TA, TK, PB.

Statistical analysis: TA, TK, PB, SV.

Drafting the manuscript: TA, PB, CL, TK.

Review of manuscript for important intellectual content: all authors.

Conflicts of Interest:

The authors declare no conflicts of interest.

Notes

All relevant data are within the paper and its Supporting Information files.

Acknowledgments & Funding Sources

This work was supported by the Convention Industrielle de Formation par la Recherche CIFRE n°2015/1111 – through the research contract between Bayer SAS, the French National Centre for Scientific Research (CNRS, CBM UPR 4301 and IAB UMR 5309, France) and Research and Development from the Association Plateforme BioPark of Archamps (France). We thank our colleagues: Dr Karim Arafah and Victor Masson, in the MassOmics group of the Association Plateforme BioPark of Archamps, for providing knowledge in LC-ESI-MS/MS and data processing, and in the preparation and processing of mycelial extracts, respectively. We also thank Stephane Peyrard and Catherine Sirven from Computational Life Science group in the La Dargoire Research Center (Bayer SAS, Lyon), for providing their expertise in protein annotation and data processing, respectively.

References

(1) Pennisi, E. Armed and Dangerous. *Science* **2010**, *327* (5967), 804–805. https://doi.org/10.1126/science.327.5967.804.

(2) Fisher, M. C.; Henk, D. A.; Briggs, C. J.; Brownstein, J. S.; Madoff, L. C.; McCraw, S. L.; Gurr, S. J. Emerging Fungal Threats to Animal, Plant and Ecosystem Health. *Nature* **2012**, *484* (7393), 186–194. https://doi.org/10.1038/nature10947.

(3) Williamson, B.; Tudzynski, B.; Tudzynski, P.; van Kan, J. A. L. Botrytis Cinerea: The Cause of Grey Mould Disease. *Mol. Plant Pathol.* **2007**, *8* (5), 561–580. https://doi.org/10.1111/j.1364-3703.2007.00417.x.
(4) van Kan, J. A. L. Licensed to Kill: The Lifestyle of a Necrotrophic Plant Pathogen. *Trends Plant Sci.* **2006**, *11* (5), 247–253. https://doi.org/10.1016/j.tplants.2006.03.005.
(5) Dean, R.; van Kan, J. A. L.; Pretorius, Z. A.; Hammond-Kosack, K. E.; Pietro, A. D.; Spanu, P. D.; Rudd, J. J.; Dickman, M.; Kahmann, R.; Ellis, J.; et al. The Top 10 Fungal Pathogens in Molecular Plant Pathology. *Mol. Plant Pathol.* **2012**, *13* (4), 414–430. https://doi.org/10.1111/j.1364-3703.2011.00783.x.
(6) Hahn, M. The Rising Threat of Fungicide Resistance in Plant Pathogenic Fungi: Botrytis as a Case Study. *J. Chem. Biol.* **2014**, *7* (4), 133–141. https://doi.org/10.1007/s12154-014-0113-1.
(7) Lucas, J. A.; Hawkins, N. J.; Fraaije, B. A. Chapter Two - The Evolution of Fungicide Resistance. In *Advances in Applied Microbiology*; Sariaslani, S., Gadd, G. M., Eds.; Academic Press, 2015; Vol. 90, pp 29–92.
(8) *Botrytis – the Fungus, the Pathogen and Its Management in Agricultural Systems*; Fillinger, S., Elad, Y., Eds.; Springer International Publishing: Cham, 2016.
(9) Brown, K. L.; Hancock, R. E. Cationic Host Defense (Antimicrobial) Peptides. *Curr. Opin. Immunol.* **2006**, *18* (1), 24–30. https://doi.org/10.1016/j.coi.2005.11.004.
(10) Cornet, B.; Bonmatin, J.-M.; Hetru, C.; Hoffmann, J. A.; Ptak, M.; Vovelle, F. Refined Three-Dimensional Solution Structure of Insect Defensin A. *Structure* **1995**, *3* (5), 435–448. https://doi.org/10.1016/S0969-2126(01)00177-0.
(11) Zhu, S.; Gao, B.; Tytgat, J. Phylogenetic Distribution, Functional Epitopes and Evolution of the CSαβ Superfamily. *Cell. Mol. Life Sci. CMLS* **2005**, *62* (19–20), 2257–2269. https://doi.org/10.1007/s00018-005-5200-6.
(12) Shafee, T. M. A.; Lay, F. T.; Hulett, M. D.; Anderson, M. A. The Defensins Consist of Two Independent, Convergent Protein Superfamilies. *Mol. Biol. Evol.* **2016**, *33* (9), 2345–2356. https://doi.org/10.1093/molbev/msw106.
(13) Vriens, K.; Cammue, B. P. A.; Thevissen, K. Antifungal Plant Defensins: Mechanisms of Action and Production. *Molecules* **2014**, *19* (8), 12280–12303. https://doi.org/10.3390/molecules190812280.
(14) Bulet, P.; Stöcklin, R. Insect Antimicrobial Peptides: Structures, Properties and Gene Regulation. *Protein Pept. Lett.* **2005**, *12* (1), 3–11.
(15) Fehlbaum, P.; Bulet, P.; Michaut, L.; Lagueux, M.; Broekaert, W. F.; Hetru, C.; Hoffmann, J. A. Insect Immunity: Septic Injury of Drosophila Induces the Synthesis of a Potent Antifungal Peptide with Sequence Homology to Plant Antifungal Peptides. *J. Biol. Chem.* **1994**, *269* (52), 33159–33163.
(16) Landon, C.; Sodano, P.; Hetru, C.; Hoffmann, J.; Ptak, M. Solution Structure of Drosomycin, the First Inducible Antifungal Protein from Insects. *Protein Sci.* **1997**, *6* (9), 1878–1884. https://doi.org/10.1002/pro.5560060908.
(17) Lamberty, M.; Ades, S.; Uttenweiler-Joseph, S.; Brookhart, G.; Bushey, D.; Hoffmann, J. A.; Bulet, P. Insect Immunity: Isolation from the Lepidopteran Heliothis Virescens of a Novel Insect Defensin with Potent Antifungal Activity. *J. Biol. Chem.* **1999**, *274* (14), 9320–9326. https://doi.org/10.1074/jbc.274.14.9320.
(18) Lamberty, M.; Caille, A.; Landon, C.; Tassin-Moindrot, S.; Hetru, C.; Bulet, P.; Vovelle, F. Solution Structures of the Antifungal Heliomicin and a Selected Variant with Both

Antibacterial and Antifungal Activities. *Biochemistry* **2001**, *40* (40), 11995–12003. https://doi.org/10.1021/bi0103563.
(19) Lamberty, M.; Zachary, D.; Lanot, R.; Bordereau, C.; Robert, A.; Hoffmann, J. A.; Bulet, P. Insect Immunity. Constitutive Expression of a Cysteine-Rich Antifungal and a Linear Antibacterial Peptide in a Termite Insect. *J. Biol. Chem.* **2001**, *276* (6), 4085–4092. https://doi.org/10.1074/jbc.M002998200.
(20) Da Silva, P.; Jouvensal, L.; Lamberty, M.; Bulet, P.; Caille, A.; Vovelle, F. Solution Structure of Termicin, an Antimicrobial Peptide from the Termite Pseudacanthotermes Spiniger. *Protein Sci.* **2003**, *12* (3), 438–446. https://doi.org/10.1110/ps.0228303.
(21) Schuhmann, B.; Seitz, V.; Vilcinskas, A.; Podsiadlowski, L. Cloning and Expression of Gallerimycin, an Antifungal Peptide Expressed in Immune Response of Greater Wax Moth Larvae, Galleria Mellonella. *Arch. Insect Biochem. Physiol.* **2003**, *53* (3), 125–133. https://doi.org/10.1002/arch.10091.
(22) Landon, C.; Barbault, F.; Legrain, M.; Menin, L.; Guenneugues, M.; Schott, V.; Vovelle, F.; Dimarcq, J.-L. Lead Optimization of Antifungal Peptides with 3D NMR Structures Analysis. *Protein Sci.* **2004**, *13* (3), 703–713. https://doi.org/10.1110/ps.03404404.
(23) Banzet, N.; Latorse, M.-P.; Bulet, P.; François, E.; Derpierre, C.; Dubald, M. Expression of Insect Cystein-Rich Antifungal Peptides in Transgenic Tobacco Enhances Resistance to a Fungal Disease. *Plant Sci.* **2002**, *162* (6), 995–1006. https://doi.org/10.1016/S0168-9452(02)00053-5.
(24) Thevissen, K.; Kristensen, H.-H.; Thomma, B. P. H. J.; Cammue, B. P. A.; François, I. E. J. A. Therapeutic Potential of Antifungal Plant and Insect Defensins. *Drug Discov. Today* **2007**, *12* (21), 966–971. https://doi.org/10.1016/j.drudis.2007.07.016.
(25) Andrès, E. Cationic Antimicrobial Peptides in Clinical Development, with Special Focus on Thanatin and Heliomicin. *Eur. J. Clin. Microbiol. Infect. Dis.* **2012**, *31* (6), 881–888. https://doi.org/10.1007/s10096-011-1430-8.
(26) Halpern, N. Entomed mise sur le système immunitaire des insectes pour soigner l'homme. *Les Echos*. December 11, 2001.
(27) Aerts, A. M.; François, I. E. J. A.; Cammue, B. P. A.; Thevissen, K. The Mode of Antifungal Action of Plant, Insect and Human Defensins. *Cell. Mol. Life Sci.* **2008**, *65* (13), 2069–2079. https://doi.org/10.1007/s00018-008-8035-0.
(28) Thevissen, K.; Warnecke, D. C.; François, I. E. J. A.; Leipelt, M.; Heinz, E.; Ott, C.; Zähringer, U.; Thomma, B. P. H. J.; Ferket, K. K. A.; Cammue, B. P. A. Defensins from Insects and Plants Interact with Fungal Glucosylceramides. *J. Biol. Chem.* **2004**, *279* (6), 3900–3905. https://doi.org/10.1074/jbc.M311165200.
(29) Landon, C.; Vovelle, F.; Sodano, P.; Pajon, A. The Active Site of Drosomycin, a Small Insect Antifungal Protein, Delineated by Comparison with the Modeled Structure of Rs-AFP2, a Plant Antifungal Protein. *J. Pept. Res.* **2000**, *56* (4), 231–238. https://doi.org/10.1034/j.1399-3011.2000.00757.x.
(30) Gao, B.; Zhu, S.-Y. Differential Potency of Drosomycin to Neurospora Crassa and Its Mutant: Implications for Evolutionary Relationship between Defensins from Insects and Plants. *Insect Mol. Biol.* **2008**, *17* (4), 405–411. https://doi.org/10.1111/j.1365-2583.2008.00810.x.
(31) Rautenbach, M.; Troskie, A. M.; Vosloo, J. A. Antifungal Peptides: To Be or Not to Be Membrane Active. *Biochimie* **2016**, *130*, 132–145. https://doi.org/10.1016/j.biochi.2016.05.013.

(32) Cools, T. L.; Struyfs, C.; Cammue, B. P.; Thevissen, K. Antifungal Plant Defensins: Increased Insight in Their Mode of Action as a Basis for Their Use to Combat Fungal Infections. *Future Microbiol*. **2017**, *12* (5), 441–454. https://doi.org/10.2217/fmb-2016-0181.

(33) El-Mounadi, K.; Islam, K. T.; Hernández-Ortiz, P.; Read, N. D.; Shah, D. M. Antifungal Mechanisms of a Plant Defensin MtDef4 Are Not Conserved between the Ascomycete Fungi Neurospora Crassa and Fusarium Graminearum. *Mol. Microbiol.* **2016**, *100* (3), 542–559. https://doi.org/10.1111/mmi.13333.

(34) Parisi, K.; Shafee, T. M. A.; Quimbar, P.; van der Weerden, N. L.; Bleackley, M. R.; Anderson, M. A. The Evolution, Function and Mechanisms of Action for Plant Defensins. *Semin. Cell Dev. Biol.* **2018**. https://doi.org/10.1016/j.semcdb.2018.02.004.

(35) Amselem, J.; Cuomo, C. A.; van Kan, J. A. L.; Viaud, M.; Benito, E. P.; Couloux, A.; Coutinho, P. M.; Vries, R. P. de; Dyer, P. S.; Fillinger, S.; et al. Genomic Analysis of the Necrotrophic Fungal Pathogens Sclerotinia Sclerotiorum and Botrytis Cinerea. *PLOS Genet*. **2011**, *7* (8), e1002230. https://doi.org/10.1371/journal.pgen.1002230.

(36) González-Fernández, R.; Aloria, K.; Valero-Galván, J.; Redondo, I.; Arizmendi, J. M.; Jorrín-Novo, J. V. Proteomic Analysis of Mycelium and Secretome of Different Botrytis Cinerea Wild-Type Strains. *J. Proteomics* **2014**, *97*, 195–221. https://doi.org/10.1016/j.jprot.2013.06.022.

(37) van Kan, J. A. L.; Stassen, J. H. M.; Mosbach, A.; Lee, T. A. J. V. D.; Faino, L.; Farmer, A. D.; Papasotiriou, D. G.; Zhou, S.; Seidl, M. F.; Cottam, E.; et al. A Gapless Genome Sequence of the Fungus Botrytis Cinerea. *Mol. Plant Pathol.* **2017**, *18* (1), 75–89. https://doi.org/10.1111/mpp.12384.

(38) Staats, M.; van Kan, J. A. L. Genome Update of Botrytis Cinerea Strains B05.10 and T4. *Eukaryot. Cell* **2012**, *11* (11), 1413–1414. https://doi.org/10.1128/EC.00164-12.

(39) Liñeiro, E.; Cantoral, J. M.; Fernández-Acero, F. J. Contribution of Proteomics Research to Understanding Botrytis Biology and Pathogenicity. In *Botrytis – the Fungus, the Pathogen and its Management in Agricultural Systems*; 2016; pp 315–333.

(40) Fernández-Acero, F. J.; Jorge, I.; Calvo, E.; Vallejo, I.; Carbú, M.; Camafeita, E.; Garrido, C.; López, J. A.; Jorrin, J.; Cantoral, J. M. Proteomic Analysis of Phytopathogenic Fungus Botrytis Cinerea as a Potential Tool for Identifying Pathogenicity Factors, Therapeutic Targets and for Basic Research. *Arch. Microbiol.* **2007**, *187* (3), 207–215. https://doi.org/10.1007/s00203-006-0188-3.

(41) González-Fernández, R.; Valero-Galván, J.; Gómez-Gálvez, F. J.; Jorrín-Novo, J. V. Unraveling the in Vitro Secretome of the Phytopathogen Botrytis Cinerea to Understand the Interaction with Its Hosts. *Front. Plant Sci.* **2015**, *6*. https://doi.org/10.3389/fpls.2015.00839.

(42) Shah, P.; Atwood, J. A.; Orlando, R.; El Mubarek, H.; Podila, G. K.; Davis, M. R. Comparative Proteomic Analysis of Botrytis Cinerea Secretome. *J. Proteome Res.* **2009**, *8* (3), 1123–1130. https://doi.org/10.1021/pr8003002.

(43) Hou, Y.; Zheng, Z.; Xu, S.; Chen, C.; Zhou, M. Proteomic Analysis of Fusarium Graminearum Treated by the Fungicide JS399-19. *Pestic. Biochem. Physiol.* **2013**, *107* (1), 86–92. https://doi.org/10.1016/j.pestbp.2013.05.009.

(44) Tanaka, S. Nutrition of Piricularia Oryzae in Vitro. In *The rice blast disease*; IRRI-Johns Hopkins Press: Baltimore, MD, 1965; pp 23–34.

(45) Ou, S. H. *Rice Diseases*, 2nd ed.; Commonwealth Mycological Institute: Kew, Surrey, UK, 1985.
(46) Strohalm, M.; Kavan, D.; Novák, P.; Volný, M.; Havlíček, V. MMass 3: A Cross-Platform Software Environment for Precise Analysis of Mass Spectrometric Data. *Anal. Chem.* **2010**, *82* (11), 4648–4651. https://doi.org/10.1021/ac100818g.
(47) Masson, V.; Arafah, K.; Voisin, S.; Bulet, P. Comparative Proteomics Studies of Insect Cuticle by Tandem Mass Spectrometry: Application of a Novel Proteomics Approach to the Pea Aphid Cuticular Proteins. *PROTEOMICS* **2018**, *18* (3–4), 1700368. https://doi.org/10.1002/pmic.201700368.
(48) Pisani, C.; Voisin, S.; Arafah, K.; Durand, P.; Perrard, M.-H.; Guichaoua, M.-R.; Bulet, P.; Prat, O. Ex Vivo Assessment of Testicular Toxicity Induced by Carbendazim and Iprodione, Alone or in a Mixture. *ALTEX - Altern. Anim. Exp.* **2016**, *33* (4), 393–413. https://doi.org/10.14573/altex.1601253.
(49) Eng, J. K.; McCormack, A. L.; Yates, J. R. An Approach to Correlate Tandem Mass Spectral Data of Peptides with Amino Acid Sequences in a Protein Database. *J. Am. Soc. Mass Spectrom.* **1994**, *5* (11), 976–989. https://doi.org/10.1016/1044-0305(94)80016-2.
(50) Kersey, P. J.; Allen, J. E.; Allot, A.; Barba, M.; Boddu, S.; Bolt, B. J.; Carvalho-Silva, D.; Christensen, M.; Davis, P.; Grabmueller, C.; et al. Ensembl Genomes 2018: An Integrated Omics Infrastructure for Non-Vertebrate Species. *Nucleic Acids Res.* **2018**, *46* (D1), D802–D808. https://doi.org/10.1093/nar/gkx1011.
(51) Käll, L.; Canterbury, J. D.; Weston, J.; Noble, W. S.; MacCoss, M. J. Semi-Supervised Learning for Peptide Identification from Shotgun Proteomics Datasets. *Nat. Methods* **2007**, *4* (11), 923–925. https://doi.org/10.1038/nmeth1113.
(52) Käll, L.; Storey, J. D.; Noble, W. S. Qvality: Non-Parametric Estimation of q-Values and Posterior Error Probabilities. *Bioinformatics* **2009**, *25* (7), 964–966. https://doi.org/10.1093/bioinformatics/btp021.
(53) Estabrook, R. W. Studies of Oxidative Phosphorylation with Potassium Ferricyanide as Electron Acceptor. *J. Biol. Chem.* **1961**, *236* (11), 3051–3057.
(54) Terras, F. R.; Schoofs, H. M.; Bolle, M. F. D.; Leuven, F. V.; Rees, S. B.; Vanderleyden, J.; Cammue, B. P.; Broekaert, W. F. Analysis of Two Novel Classes of Plant Antifungal Proteins from Radish (Raphanus Sativus L.) Seeds. *J. Biol. Chem.* **1992**, *267* (22), 15301–15309.
(55) Nanni, V.; Schumacher, J.; Giacomelli, L.; Brazzale, D.; Sbolci, L.; Moser, C.; Tudzynski, P.; Baraldi, E. VvAMP2, a Grapevine Flower-Specific Defensin Capable of Inhibiting Botrytis Cinerea Growth: Insights into Its Mode of Action. *Plant Pathol.* **2014**, *63* (4), 899–910. https://doi.org/10.1111/ppa.12170.
(56) Thevissen, K.; Terras, F. R. G.; Broekaert, W. F. Permeabilization of Fungal Membranes by Plant Defensins Inhibits Fungal Growth. *Appl. Environ. Microbiol.* **1999**, *65* (12), 5451–5458.
(57) Osborn, R. W.; Samblanx, G. W. D.; Thevissen, K.; Goderis, I.; Torrekens, S.; Leuven, F. V.; Attenborough, S.; Rees, S. B.; Broekaert, W. F. Isolation and Characterisation of Plant Defensins from Seeds of Asteraceae, Fabaceae, Hippocastanaceae and Saxifragaceae. *FEBS Lett.* **1995**, *368* (2), 257–262. https://doi.org/10.1016/0014-5793(95)00666-W.
(58) Broekaert, W. F.; Terras, F.; Cammue, B.; Osborn, R. W. Plant Defensins: Novel Antimicrobial Peptides as Components of the Host Defense System. *Plant Physiol.* **1995**, *108* (4), 1353–1358. https://doi.org/10.1104/pp.108.4.1353.

(59) Spelbrink, R. G.; Dilmac, N.; Allen, A.; Smith, T. J.; Shah, D. M.; Hockerman, G. H. Differential Antifungal and Calcium Channel-Blocking Activity among Structurally Related Plant Defensins. *Plant Physiol.* **2004**, *135* (4), 2055–2067. https://doi.org/10.1104/pp.104.040873.

(60) Schulthess, B.; Ledermann, R.; Mouttet, F.; Zbinden, A.; Bloemberg, G. V.; Böttger, E. C.; Hombach, M. Use of the Bruker MALDI Biotyper for Identification of Molds in the Clinical Mycology Laboratory. *J. Clin. Microbiol.* **2014**, *52* (8), 2797–2803. https://doi.org/10.1128/JCM.00049-14.

(61) Thevissen, K.; Tavares, P. de M.; Xu, D.; Blankenship, J.; Vandenbosch, D.; Idkowiak-Baldys, J.; Govaert, G.; Bink, A.; Rozental, S.; Groot, P. W. J. de; et al. The Plant Defensin RsAFP2 Induces Cell Wall Stress, Septin Mislocalization and Accumulation of Ceramides in Candida Albicans. *Mol. Microbiol.* **2012**, *84* (1), 166–180. https://doi.org/10.1111/j.1365-2958.2012.08017.x.

(62) Funato, K.; Riezman, H. Vesicular and Nonvesicular Transport of Ceramide from ER to the Golgi Apparatus in Yeast. *J. Cell Biol.* **2001**, *155* (6), 949–960. https://doi.org/10.1083/jcb.200105033.

(63) Hayes, B. M. E.; Bleackley, M. R.; Anderson, M. A.; Van der Weerden, N. L. The Plant Defensin NaD1 Enters the Cytoplasm of Candida Albicans via Endocytosis. *J. Fungi* **2018**, *4* (1), 20. https://doi.org/10.3390/jof4010020.

1048 **For Table of Contents Only**

1049

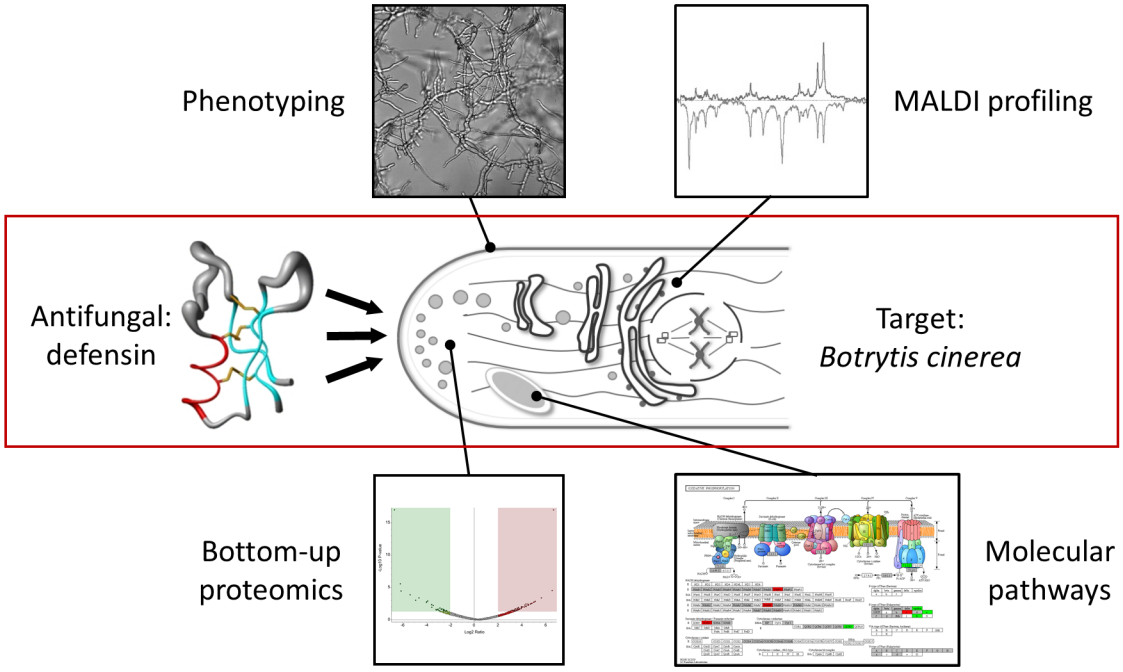

1050